Available online at www.sciencedirect.com

ScienceDirect

Geochimica et Cosmochimica Acta 183 (2016) 153–175

Geochimica et Cosmochimica Acta

www.elsevier.com/locate/gca

The role of skeletal micro-architecture in diagenesis and dating of *Acropora palmata*

P.J. Tomiak [a], M.B. Andersen [a,b,*], E.J. Hendy [a,c], E.K. Potter [b], K.G. Johnson [d], K.E.H. Penkman [e]

[a] *School of Earth Sciences, University of Bristol, Bristol BS8 1RJ, United Kingdom*
[b] *Insitute of Geochemistry and Petrology, Department of Earth Sciences, ETH Zürich, CH 8092 Zürich, Switzerland*
[c] *School of Biological Sciences, University of Bristol, Bristol BS8 1UG, United Kingdom*
[d] *Department of Earth Sciences, The Natural History Museum, Cromwell Road, London SW7 5BD, United Kingdom*
[e] *BioArCh, Department of Chemistry, University of York, York YO10 5DD, United Kingdom*

Received 31 July 2015; accepted in revised form 25 March 2016; Available online 06 April 2016

Abstract

Past variations in global sea-level reflect continental ice volume, a crucial factor for understanding the Earth's climate system. The Caribbean coral *Acropora palmata* typically forms dense stands in very shallow water and therefore fossil samples mark past sea-level. Uranium-series methods are commonly used to establish a chronology for fossil coral reefs, but are compromised by post mortem diagenetic changes to coral skeleton. Current screening approaches are unable to identify all altered samples, whilst models that attempt to correct for 'open-system' behaviour are not applicable across all diagenetic scenarios. In order to better understand how U-series geochemistry varies spatially with respect to diagenetic textures, we examine these aspects in relation to skeletal micro-structure and intra-crystalline amino acids, comparing an unaltered modern coral with a fossil *A. palmata* colony containing zones of diagenetic alteration (secondary overgrowth of aragonite, calcite cement and dissolution features). We demonstrate that the process of skeletogenesis in *A. palmata* causes heterogeneity in porosity, which can account for the observed spatial distribution of diagenetic features; this in turn explains the spatially-systematic trends in U-series geochemistry and consequently, U-series age. We propose a scenario that emphasises the importance of through-flow of meteoric waters, invoking both U-loss and absorption of mobilised U and Th daughter isotopes. We recommend selective sampling of low porosity *A. palmata* skeleton to obtain the most reliable U-series ages. We demonstrate that intra-crystalline amino acid racemisation (AAR) can be applied as a relative dating tool in Pleistocene *A. palmata* samples that have suffered heavy dissolution and are therefore unsuitable for U-series analyses. Based on relatively high intra-crystalline concentrations and appropriate racemisation rates, glutamic acid and valine are most suited to dating mid-late Pleistocene *A. palmata*. Significantly, the best-preserved material in the fossil specimen yields a U-series age of 165 ± 8 ka, recording a paleo sea-level of -35 ± 7 msl during the MIS 6.5 interstadial on Barbados.

Keywords: Coral; U-series dating; Amino acid racemisation; Diagenesis; Skeletogenesis; Sea-level; MIS 6.5

1. INTRODUCTION

The elk horn coral *Acropora palmata* is a useful proxy for past sea-level because it has a very limited depth range, with dense stands developing in or just below the breaker

* Corresponding author at: School of Earth & Ocean Sciences, Cardiff University, Main Building, Room 2.54, Park Place, Cardiff CF10 3AT, United Kingdom. Tel.: +44 29 208 74943.
E-mail address: AndersenM1@cardiff.ac.uk (M.B. Andersen).

http://dx.doi.org/10.1016/j.gca.2016.03.030
0016-7037/

zone (Lighty et al., 1982), and was common in Quaternary fossil reefs of the Caribbean. Sea-level reconstructions based on fossils require a robust chronology, and U-series dating provides the most precise approach for Quaternary corals (as reviewed in Stirling and Andersen, 2009). The most commonly used U-series dating technique assumes that decay of the ^{238}U parent nuclide into its longest-lived intermediate radioactive daughter nuclides, ^{234}U and ^{230}Th, occurs within a closed system. This assumption is often compromised by diagenetic alteration of the aragonitic skeleton (e.g. Hamelin et al., 1991). Diagenesis can involve loss of mineral (dissolution) and preferential leaching of certain elements (e.g. Schroeder, 1969; Hendy et al., 2007), addition of new material (cementation) of the same or different mineralogy (e.g. Nothdurft and Webb, 2009), and/or replacement of primary material (e.g. Scherer, 1974; Cusack et al., 2008). The rigidity and porosity of coral skeletons increases susceptibility to diagenesis by promoting fluid circulation (e.g. Constantz, 1986; Dullo, 1987). *A. palmata* is particularly susceptible to these diagenetic changes and the consequent occurrence of inaccurate U-series ages has led to a preference for other, apparently less sensitive, species (e.g. Stirling et al., 1995, 1998; Andersen et al., 2008). The advantage of using *A. palmata*, for this study is twofold: (1) the potential to improve reliable dating capabilities of this coral species given its superiority as a sea-level marker compared to most other coral species and (2) the susceptibility to diagenesis, together with the characteristic internal variability in *A. palmata* microstructure, make this species an excellent candidate for investigating the general open-system U-series systematics that can affect all corals during diagenetic alteration.

Current techniques used to screen altered material prior to U-series isotopic analysis cannot identify all samples exhibiting open-system behaviour (e.g. Bar-Matthews et al., 1993; Fruijtier et al., 2000; Scholz et al., 2007; Andersen et al., 2008). Consequently, various 'post-analytical' methods, such as comparing decay-corrected $^{234}U/^{238}U$ in fossil corals to that of modern counterparts, have been used to identify compromised samples (e.g. Hamelin et al., 1991; Gallup et al., 1994; Stirling et al., 1995). Further attempts to obtain reliable U-series ages from fossil corals have steered towards modelling and correcting for open-system behaviour (e.g. Thompson et al., 2003). Typically, open-system U-series corrections are based solely on post-analytical geochemical observations (e.g. Thompson et al., 2003; Villemant and Feuillet, 2003; Scholz et al., 2004; Potter et al., 2004), rather than linking physical evidence of subtle diagenetic changes to the U-series system. In part, this dichotomy is a consequence of *a priori* rejection of samples with visible alteration, but sub-sampling across coevally deposited skeletal material within single diagenetically altered colonies can help isolate geochemical imprints from diagenesis (Henderson et al., 1993; Scholz and Mangini, 2007; Scholz et al., 2007; Shen et al., 2008; Andersen et al., 2010a; Obert et al., 2016), thereby improving the screening of material and enhancing the capacity for model age corrections. In addition, initial screening could include a secondary dating technique such as amino acid racemisation (AAR), to improve sample selection for U-series dating of fossil corals (Hendy et al., 2012). Recent improvements in analysis and sample preparation (e.g. Kaufman and Manley, 1998; Penkman et al., 2008) mean a re-assessment of the diagenetic sensitivity and geochronological potential of AAR in Quaternary coral, last explored by Wehmiller et al. (1976), is timely.

In this study we test the influence of coral skeletogenesis and a range of diagenetic processes on U-series geochemistry and AAR by comparing a modern and a fossil diagenetically-altered *A. palmata* colony to isolate primary micro-structural, organic (intra-crystalline amino acids) and isotopic (U-series) variability from secondary diagenetic features. We provide evidence that heterogeneity in porosity within an individual colony localises diagenetic processes, promoting spatially-systematic trends in geochemistry, with particular relevance to retrieving robust ages from *A. palmata*. By examining U-series and AAR systematics at the millimetre-scale within the fossil colony, we identify 'pristine' areas of coral skeleton in order to derive a more robust U-series age. Significantly, these results indicate that the fossil *A. palmata* colony grew during Marine Isotope Stage (MIS) 6.5, a warmer sub-stage within the MIS 6 glacial that coincided with a prominent peak in Northern Hemisphere insolation (Berger, 1978). Previous sea-level, and therefore ice-volume, estimates during this complex but climatically important interstadial indicate only a moderate sea-level high-stand compared with interglacial levels (Scholz et al., 2007; Grant et al., 2014). The duration is also uncertain (Bard et al., 2002; Thompson and Goldstein, 2005; Scholz et al., 2007). We use the data derived from the fossil *A. palmata* sample to constrain the timing and amplitude of sea-level during MIS 6.5.

2. MATERIALS AND METHODS

2.1. Coral samples

The fossil *A. palmata* sample (U6-11 K3243) was selected because it displayed spatial variability in microstructure and diagenetic alteration. It was collected in growth position at 9.8 m above current sea-level from the "Gully" sample site at Foul Bay (13°5′30″ N, 59°26′54″ W) SE coast of Barbados, between Salt Cave Point and Deebles Point (Schellmann and Radtke, 2004a; Fig. 1). Electron spin resonance (ESR) dates from *A. palmata* colonies in the same reef sequence range between 182 ± 18 and 232 ± 27 ka (Schellmann and Radtke, 2004a). A 10 mm thick slice (150 × 120 mm diameter) cut perpendicular to growth was sectioned into four transects (Fig. 2a); three of these were cut into 16 contiguous sub-samples (~6 × 9 × 10 mm) for SEM, U-series and AAR analysis (transects A–C respectively), whilst four thin sections were prepared from the fourth transect (transect D).

The modern *A. palmata* colony came from the University of Bristol's collection (collected live by Dr. Tom Thompson, Jamaica, 1974). Transverse slices were cut (Fig. 2b) from the growing tip, middle and base of the colony branch (Fig. 2c–e respectively). The central axial region (i.e. minus protruding radial corallites) was sub-sampled from the top slice, and transects were

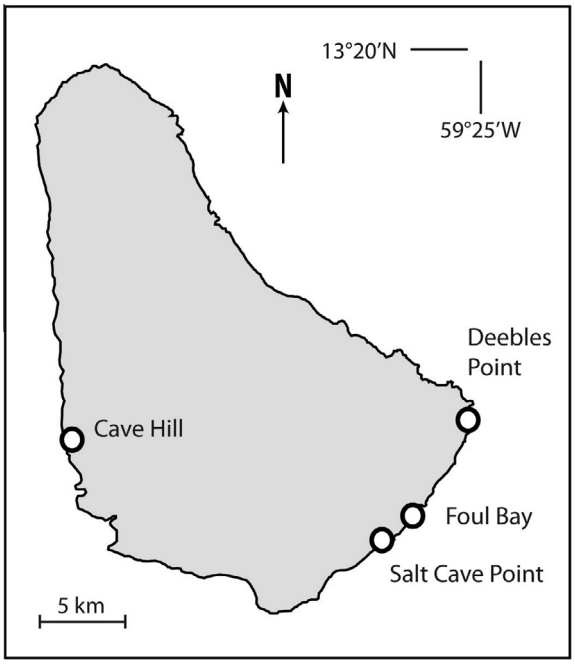

Fig. 1. Map of Barbados showing key locations.

sub-sampled (~5 × 4 × 2 mm) across mid and base slices (Fig. 2b). In addition, a sub-sample comprising radial corallites was selectively cut from a middle slice outer edge (henceforth called 'Mid corallites' sample), and sub-samples dominated by open-structure framework and dense thickened skeleton microstructure (henceforth called 'Base framework' and 'Base infilled' respectively) were collected from a base slice. A thin section of a base slice was also prepared. All sub-samples were ultra-sonicated in MilliQ >18.2 MΩ/cm deionised filtered water and air-dried. As AAR analyses are conducted on powdered samples, the skeletal material was crushed to produce a homogenous powder; this sample preparation also allowed equivalent sub-samples to be used for further chemical analyses.

2.2. Fabric analysis

Micro-structural features and diagenetic alteration were mapped using a range of visual and analytical tools. SEM imaging (secondary and backscatter) of Au-coated samples was performed using a Hitachi S-3500N variable pressure microscope. Petrolab Limited prepared thin sections, vacuum impregnating the samples with a low viscosity epoxy resin containing a yellow fluorescent dye (Figs. 2–4), and void morphology was quantified using Fiji/ImageJ 1.47 image analysis software (Schindelin et al., 2012). Thin section images were collected using a Leica M205C microscope equipped with a Leica DFC425c digital colour microscope camera.

Bulk carbonate mineralogy was determined by X-ray diffraction (XRD) on a selection of the dry powered fossil sub-samples (1, 3, 5, 9, 13 and 15; Transect B), mounted onto silicon wafer discs and scanned from $20° < 2\Theta < 70°$ on a Bruker-AXS D8 Advance Power Diffractometer (Cu-Ka radiation; 1.5418 Å, and a PSD LynxEye detector). Diffraction data was processed and evaluated using DIFFRACplus EVA analysis software, and the ICDD database. The detection limit of calcite was 1%. The distribution of secondary cement mineralogy was mapped by DXR Raman Microscope (Thermo Scientific; wavelength 532 nm, exposure time 0.5 s; 900 lines/mm grating), with spectra matched to the RRUFF database for calcite and aragonite (Downs, 2006). The false colour map (Fig. 5f) was generated by integrating the peak range (195–215 cm^{-1}) corresponding to aragonite.

2.3. U-series geochemistry

Uranium concentrations were measured in the modern *A. palmata* on a Thermo-Finnigan Element 2 ICPMS in the Bristol Isotope Group, following Andersen et al. (2013). Samples were dissolved in mixed solutions of 4 N HNO_3 – 10% H_2O_2 solution (to oxidise organic matter) then fluxed at 110 °C on a hot-plate and dried down. Samples were then re-dissolved in ~0.3 N HNO_3 to achieve [U] of ~1 ppb for ICPMS analysis. Reproducibility of the determined [U] was monitored during the sequence using replicates of an internal coral standard (<±10%, 2 SD).

U-series isotopic and [U] determinations for the fossil coral were conducted using isotope dilution and measured using a Neptune MC-ICPMS instrument (Thermo Finnigan, Germany) in the Bristol Isotope Group, using a similar protocol to Andersen et al. (2013). Each sample (~0.4 g) was fully dissolved using slow addition of high-purity HNO_3 to the sample already suspended in Milli-Q H_2O, then spiked with a ^{233}U–^{229}Th mixed tracer (see details in Andersen et al., 2008) and dried down. Sample-spike equilibration was achieved by re-dissolution using an HNO_3–H_2O_2 mixture (at 120 °C), which was subsequently dried-down. The samples were subsequently prepared in 5 ml of 3 N HNO_3 and chemical separation and purification of U and Th from the matrix was achieved using UTEVA resin (Eichrom) following the separation method outlined in Potter et al. (2005a) for the UTEVA resin. Following chemical separation, the U and Th cut of each sample were dried down, then refluxed in a HNO_3–H_2O_2 mixture (at 120 °C, to oxidise any resin bleeding into the sample) and dried down again. Finally, samples were prepared for MC-ICPMS analysis in 2 ml of 0.2 N HCl for both the U and Th cut. Full procedural blanks (from dissolution and column chemistry) had total ^{238}U and ^{232}Th concentrations <5 pg; at these low levels blank corrections were deemed unnecessary.

As outlined in Andersen et al. (2013) the MC-ICPMS analysis consisted of three separate sequences, cycling the minor isotopes (^{234}U, ^{233}U, ^{230}Th, ^{229}Th) in the central secondary electron multiplier (SEM). In sequence (1) and (2), ^{234}U and ^{233}U were collected in the SEM, respectively, whilst ^{235}U and ^{238}U were collected simultaneously in Faraday cups equipped with 10^{11} ohm resistors. In sequence (3) ^{229}Th and ^{230}Th were cycled through the SEM using a "peak jumping" routine and ^{232}Th isotopes were collected simultaneously in Faraday cups equipped with 10^{11} ohm resistors during both cycles. During analyses each sample/standard was background-corrected using average values from the preceding on-peak 0.2 N HCl blank measure-

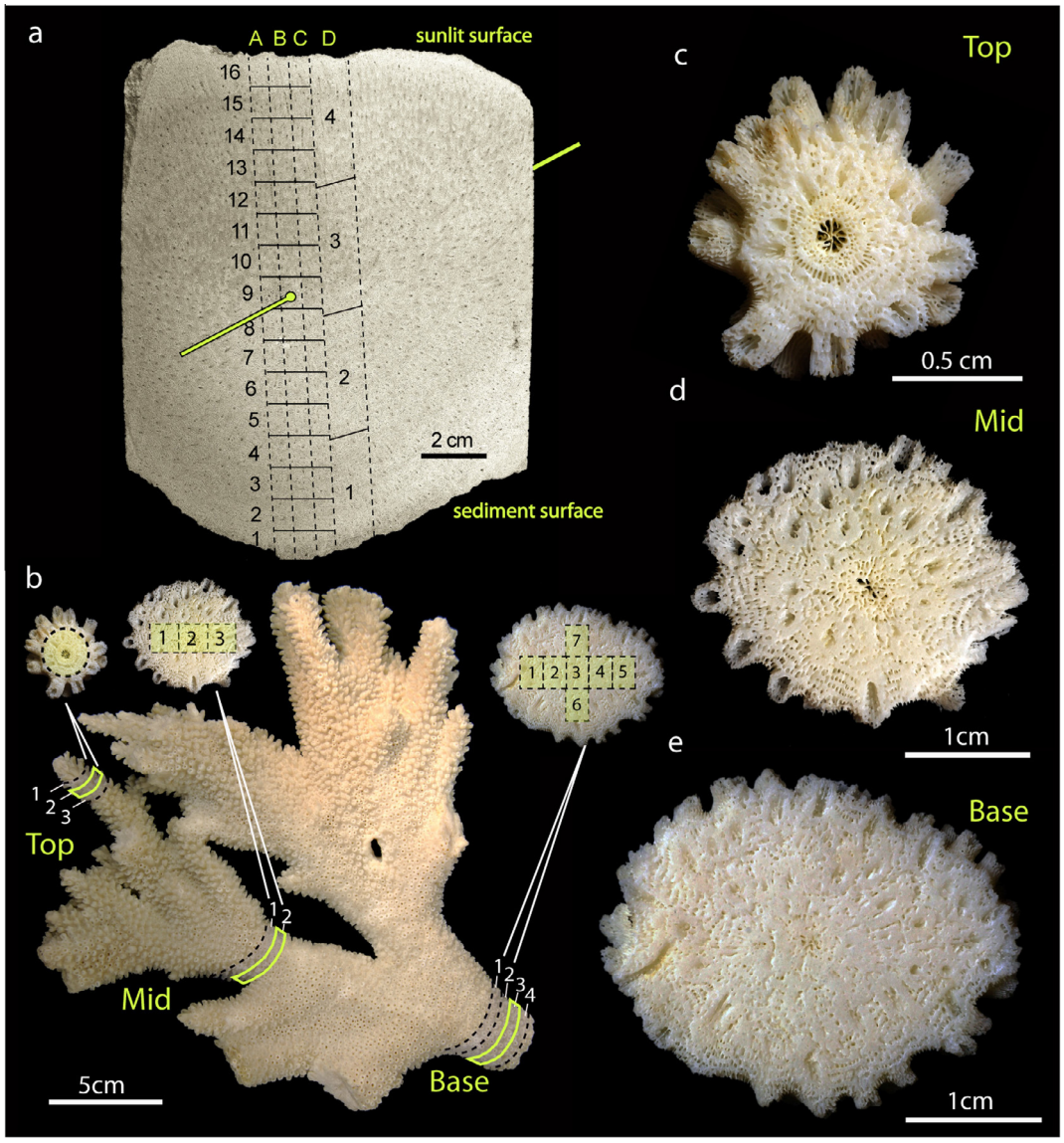

Fig. 2. Photographic images of fossil (a) and modern (b–e) *Acropora palmata* showing sample slices and sub-sampling transects.(a) Fossil *A. palmata* slice (U6-11 K3243), transect A for SEM, B for U-series and X-ray diffraction (XRD), C for AA composition and racemisation (~6 × 9 × 10 mm), and D for thin sections. Approximate growth axis is indicated by the yellow line. (b) Modern *A. palmata* colony (U. Bristol collection) with slices (~5 × 4 × 2 mm) enlarged in (c), (d) and (e) from the top (~2 cm from growing tip), middle (~8 cm) and base (~20 cm) of the modern colony respectively. All slices are orientated in figure with the sunlit-surface facing skeleton at top. (For interpretation of the references to colour in this figure legend, the reader is referred to the web version of this article.)

ments. These corrections were negligible (<0.05‰ of the on-peak measurement for the U isotopes and ^{230}Th-^{229}Th, <0.5‰ for ^{232}Th). The ^{234}U/^{238}U and ^{233}U/^{238}U, were all corrected for spike impurities, SEM non-linearity, Faraday-SEM gain, instrumental mass bias and U tailing below ^{234}U and ^{233}U, using comparisons to bracketing standards of CRM-145 and an in-house U standard, respectively (see Andersen et al., 2013 for details).

Three minor adjustments to the procedure of Andersen et al. (2013) were conducted. Firstly, the low abundance of ^{232}Th precluded the use of this isotope for normalising ^{230}Th and ^{229}Th in each cycle, and the directly measured ^{230}Th/^{229}Th from the peak-jumping routine was used instead. Secondly, the Th isotopes were measured without admixed U for mass bias correction, instead adopting a standard bracketing method (Hoffmann et al., 2007). The Th isotopes of the unknowns were corrected for spike impurities, SEM non-linearity, and instrumental mass bias, using the off-set between the measured and the "absolute" ratio for the in-house Th standard Teddii (Hoffmann et al., 2007), which was measured interspersed in between each three unknowns. No bias was observed for the ^{230}Th/^{229}Th ratio of the Teddii standard, obtained either with or without normalising to the ^{232}Th measured in the Faraday cups during each cycle. Thirdly, an absolute ^{238}U/^{235}U value of 137.780 was used for the mass bias

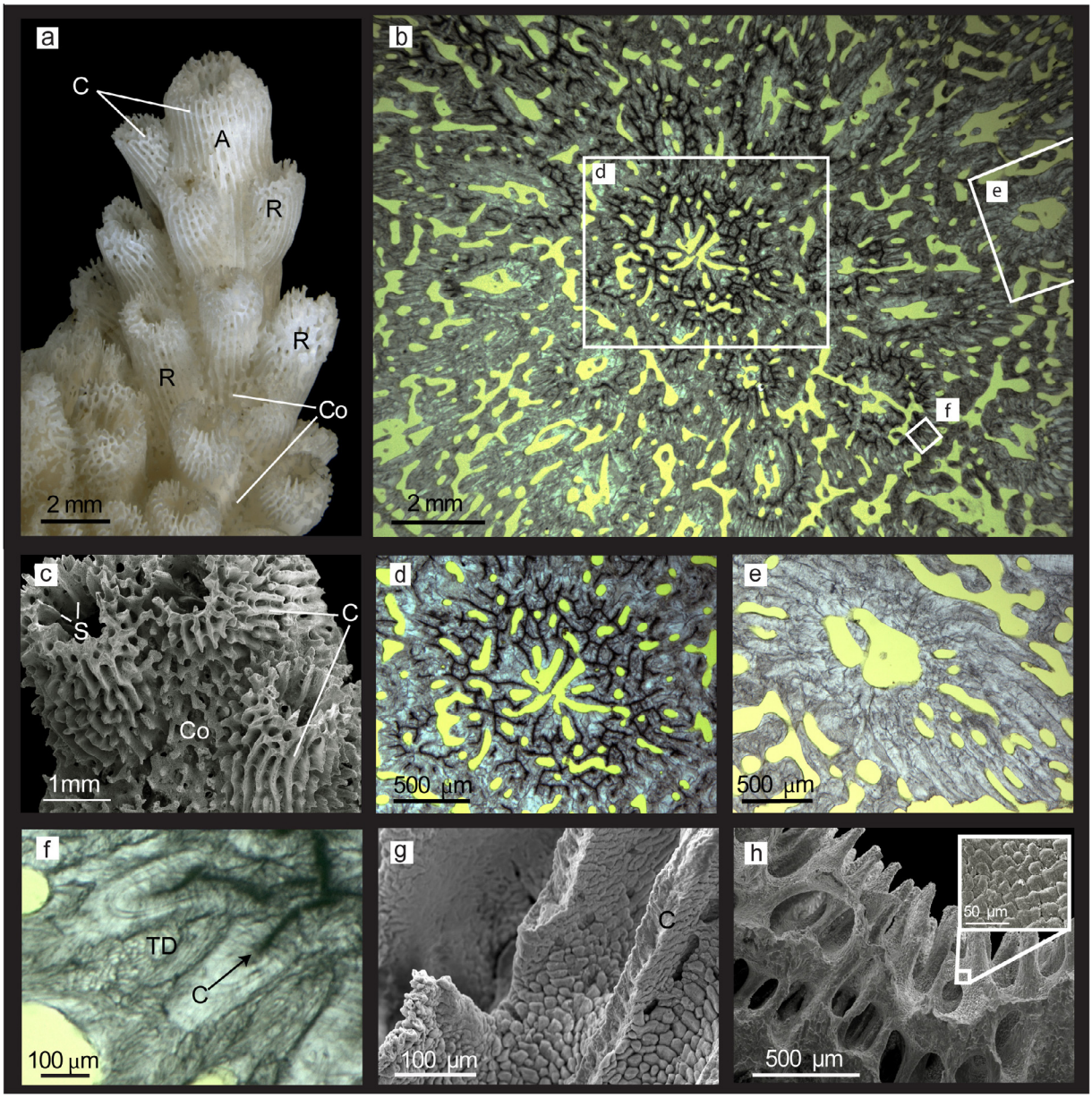

Fig. 3. Skeletal features from the modern *A. palmata* colony. Example of a branch growth tip under light microscope (a) and SEM (c). Both axial ('A') and radial ('R') corallites exhibit septae ('S') and ridges running up the side of individual corallites (costae, 'C'). Reticulate skeleton (coenosteum, 'Co') occurs between corallites. Thin section images (b, d, e, and f) are from the base slice. The axial corallite is surrounded by an inner primary ring of radial corallites (b). Axial corallites have visible dark centres of rapid accretion (CRAs) along the skeletal midline of septa and costae (b and d). Radial corallites also have CRAs in the early stage of ontogeny, when they first branch from the axial corallite (b), but these features are not evident in older radial corallites (b and e) greater than ~6 mm from central axial corallite. Incremental skeletal growth is visible on costae (f) with thickening deposits ('TD') forming between costae ('C'). Under SEM, thickening deposits are visible as "shingles" on the skeletal surface of corallites between costae (g) and on coenosteal skeleton (h). The process of thickening may simply involve continued extension of fibre bundles (Gladfelter, 2007), or alternatively, a second distinct process of crystal growth (Nothdurft and Webb, 2007) with a different chemical composition (Shirai et al., 2008).

correction in sequence (1) and (2) for the coral samples, a $^{238}U/^{235}U$ composition ~0.4‰ lighter than the CRM-145 standard (137.829; Hiess et al., 2012). To verify this approach two splits of the powdered sub-samples (6 and 11) were processed and measured specifically for $^{238}U/^{235}U$ using the exact sample dissolution and measurement procedure as outlined in Andersen et al. (2015). The sub-sample 6 and 11, yielded $^{238}U/^{235}U$ compositions of 137.785 ± 0.004 and 137.774 ± 0.004 (2 SD), respectively, justifying the used "absolute" $^{238}U/^{235}U$ ratio (137.780) for all the coral sub-samples.

Isotopic ratios were reformulated into activity ratios (which can determined from the measured atomic ratio of the isotopes in question multiplied by the ratio of their

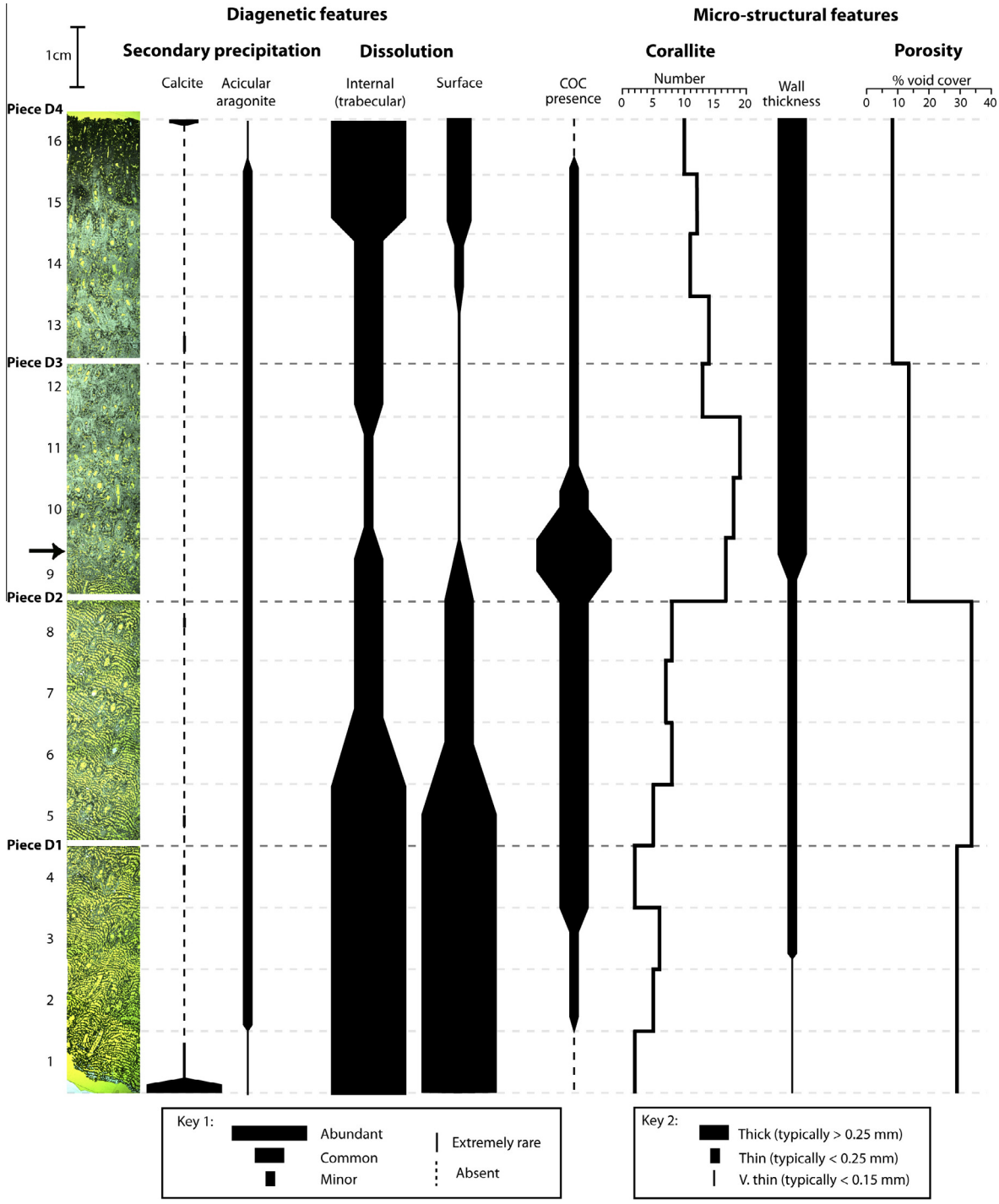

Fig. 4. The spatial distribution of skeletal diagenetic and micro-structural features in the fossil *A. palmata* colony. Thin sections (transect D; Fig. 1a) orientated in "life position" (bottom = lower sediment-facing surface, top = upper surface); numbers up the left hand side match the numbering of transect A, B and C sub-sample pieces. The extent of secondary precipitation was estimated from examination of thin sections (e.g. Fig. 5) and confirmation by XRD and Raman microspectroscopy. Extent of dissolution was estimated from SEM and thin section observations (see examples in Fig. 5). CRA presence was estimated from thin sections (e.g. Fig. 2) and SEM of etched skeleton. The number of corallites (axial and radial) per sub-sample was determined from the thin sections; axial corallites were only distinguishable around sub-sample 9. The arrow (sub-sample 9) marks the lowest occurrence of the axial corallites and the transition from the predominantly "framework" skeleton below. Wall thickness was measured on thin sections and porosity was quantified using image analysis software (note that% void cover was calculated as an average over 4 sub-samples).

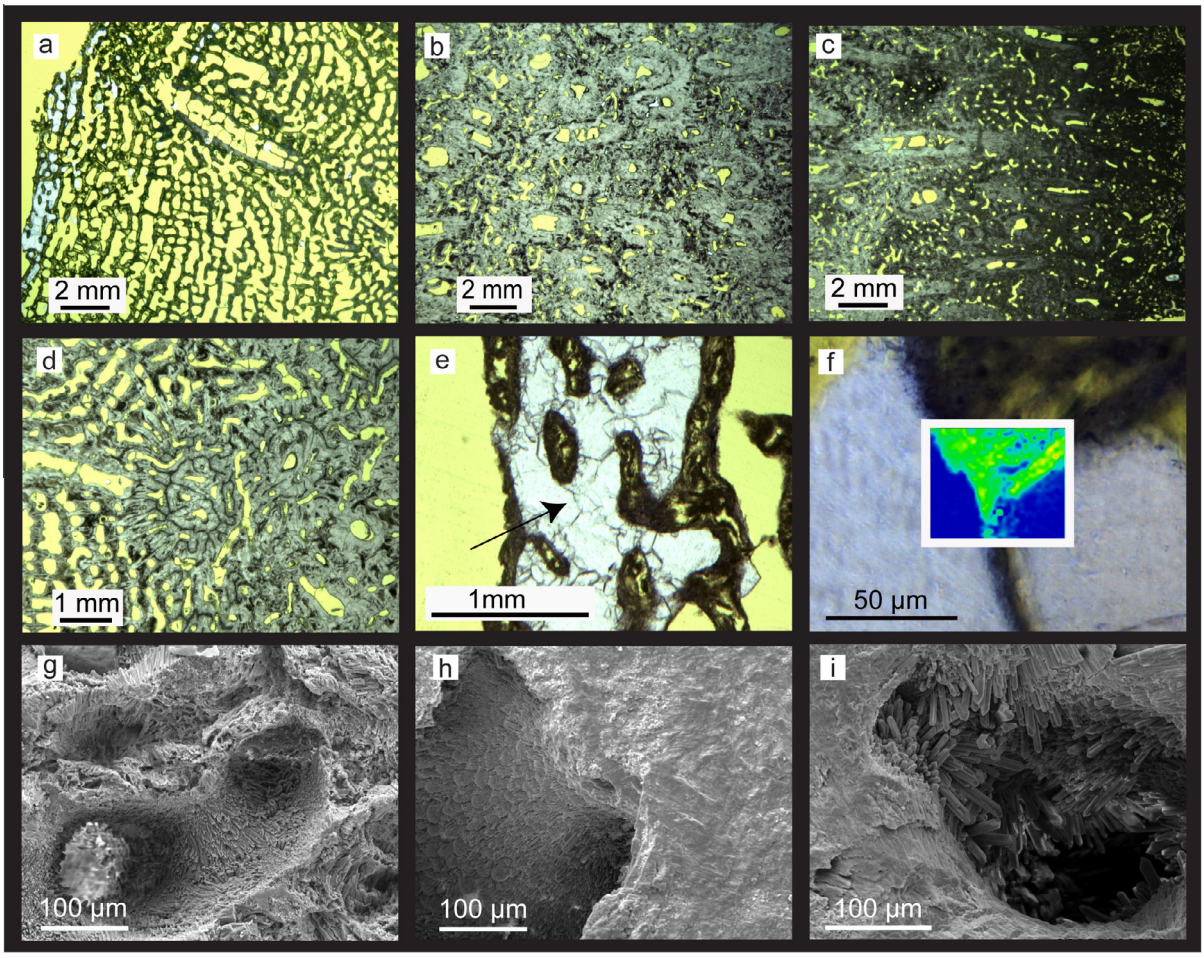

Fig. 5. Example diagenetic and micro-structural features in the fossil *A. palmata* colony. (a–c) Light-microscope thin section images in sequence from (a) lower outer edge (position sub-sample 1), (b) central/upper section (sub-sample 11/12), and (c) upper outer surface skeleton (sub-samples 15/16). (d) Higher magnification image of the axial corallite zone at the transition in skeletal density (sub-sample 9); evidence of CRAs (black "threads" along the mid-point of the axial corallite walls) is preserved in these axial corallites. (e) Calcite infilling (indicated by arrow, enlarged from a) was confirmed by Raman microspectroscopy mapping (inset f) showing calcite in blue and aragonite in yellow-green (one anomalous highly fluorescing pixel was excluded from the image). Note transition from open skeletal framework and high levels of internal dissolution at the base of the transect and fossil colony (a, SEM image g) to thicker walled axial corallites containing evidence of CRAs in the central section (d), to the radial corallite-rich dense central/upper section with both coenosteum and corallite walls (light grey) thickened (b), to the outer upper surface skeleton where dissolution of the coenosteum between corallites increases (c). The SEM image (h) from sub-sample 10 demonstrates where dissolution (internal or surface) is absent and shows the preserved "shingle" micro-structure surface (contrast with SEM image (g) at same scale with exposed individual aragonite needles due to loss of surface). (i) Example of secondary aragonite precipitation within a skeletal pore (SEM image from sub-sample 12).

decay constants) and the $[^{234}U/^{238}U]_{act}$ are expressed in delta notation ($\delta^{234}U$), representing the permil (parts per thousand) deviation away from secular equilibrium:

$$\delta^{234}U(‰) = \left\{ \left(\frac{^{234}U/^{238}U_{sample}}{^{234}U/^{238}U_{sec.eq.}} \right) - 1 \right\} \times 10^3 \quad (1)$$

where $(^{234}U/^{238}U)_{sample}$ is the measured atomic ratio and $(^{234}U/^{238}U)_{sec.eq.}$ is the atomic ratio at secular equilibrium. The decay constants used were those reported by Cheng et al. (2000); $\lambda_{234} = 2.8262 \times 10^{-6}\,y^{-1}$, $\lambda_{230} = 9.158 \times 10^{-6}\,y^{-1}$, and $\lambda_{238} = 1.551 \times 10^{-10}\,y^{-1}$. New half-life estimates have recently been published (Cheng et al., 2013); although within the range of the Cheng et al. (2000) estimates, the main difference using the Cheng et al. (2013) calibration would be that the reported $\delta^{234}U$ values are shifted 1.2‰ higher. However, these readjustments are generally within the uncertainty measurements and the estimates from Cheng et al. (2000) are used here, to make the measurements presented in this study directly comparable with previously published studies.

The following equation (Broecker, 1963) was used to calculate a U-series age for a sample:

$$1 - \left[\frac{^{230}Th}{^{238}U} \right]_{act} = e^{-\lambda_{230} t} - \left(\frac{\delta^{234}U}{1000} \right) \left(\frac{\lambda_{230}}{\lambda_{230} - \lambda_{234}} \right) (1 - e^{(\lambda_{234} - \lambda_{230})t}) \quad (2)$$

If the $^{230}Th/^{238}U$ and $^{234}U/^{238}U$ ratios can be reliably measured, then only t (the age in years) remains unknown. As t appears twice, the equation has to be solved by iteration. This calculation assumes that (a) initial thorium

concentrations are zero (and therefore initial $^{230}Th/^{238}U = 0$), (b) that no significant ^{238}U decay has occurred over the period of interest, and (c) that any changes in isotopic ratios are purely a consequence of decay and ingrowth.

The analytical performance, reproducibility and accuracy of the method were tested using four replicates each of powdered coral samples NB-C-2 (Henderson Island) and AC-1 (Australian National University) compared to previous high-precision measurements on large sample sizes in Andersen et al. (2008, 2010a). These measurements of NB-C-2 yielded $\delta^{234}U = 80.1 \pm 2.4‰$ and $[^{230}Th/^{238}U]_{act} = 0.9821 \pm 0.0028$ (2 SD) in good agreement with the $\delta^{234}U$ of $78.9 \pm 0.3‰$ and $[^{230}Th/^{238}U]_{act}$ of 0.9786 ± 0.0004 (2 SD) reported in Andersen et al. (2010a). Similarly, AC-1 gave a $\delta^{234}U$ of $103.0 \pm 1.4‰$ and $[^{230}Th/^{238}U]_{act}$ of 0.7625 ± 0.0015 (2 SD) again in good agreement with $\delta^{234}U = 102.9 \pm 0.3‰$ and $[^{230}Th/^{238}U]_{act} = 0.7609 \pm 0.0003$ (2 SD) reported in Andersen et al. (2008).

2.4. Organic geochemistry: amino acid composition and racemisation

Coral sub-samples were analysed for amino acid (AA) composition and racemisation on the isolated 'intra-crystal line' AA fraction following Hendy et al. (2012). Splits of homogenised powdered samples were prepared as full-procedural duplicates; variability was expressed using 95% confidence interval repeatability (CIR) error bars (Electronic Annex, EA, Eq. (EA 1)). Reverse-phase high-pressure liquid chromatography (RP-HPLC) analyses of both the free amino acids (FAA) and total hydrolysable amino acid (THAA) fractions for each sample were conducted following Penkman et al. (2008). The FAA fraction is the naturally hydrolysed (free) AAs released from proteins over time through peptide bond hydrolysis. Exposing samples to concentrated mineral acid at high temperature (20 μL 7 M HCl per mg of sample, under N_2 at 110 °C for 24 h) hydrolyses residual peptide bonds and allows the total hydrolysable AA (THAA) fraction to be measured. During preparative hydrolysis asparagine (Asn) and glutamine (Gln) undergo rapid irreversible deamidation into aspartic acid (Asp), and glutamic acid (Glu) respectively (Hill, 1965; Goodfriend, 1991; Brinton and Bada, 1995). Asp and Asn are therefore reported collectively as aspartic acid (Asx), and Gln and Glu as glutamic acid (Glx). Both L and D enantiomer concentrations were determined for aspartic acid (Asx), glutamic acid (Glx), serine (Ser), alanine (Ala), valine (Val), phenylalanine (Phe), leucine (Leu) and isoleucine (Ile). The total AA concentration ([total]) represents the sum of these individual AAs measured in the THAA fraction. This same suite of amino acids was used to express AA composition, the relative contribution of each given as mol% AA ([AA]/[total] × 100).

Isothermal heating experiments were used to examine whether the intra-crystalline fraction operates as a closed-system in *A. palmata*. Following Tomiak et al. (2013), powdered fossil *A. palmata* samples were bleached and heated at 140 °C under aqueous conditions for 6 ($n = 3$) or 24 ($n = 3$) hours. Both heated powder and supernatant water were analysed, with the FAA and THAA concentrations in the supernatant water (FAA_w and $THAA_w$ respectively) compared to water blanks (heated under the same conditions, but without coral powder) to monitor any leaching.

3. RESULTS

3.1. Skeletal fabric analysis

3.1.1. Modern *A. palmata* specimen

The modern specimen had the microstructure and fabric of a pristine skeleton with no evidence of dissolution or secondary mineralisation. Axial corallites were surrounded by an outgrowth of numerous protruding radial corallites (Figs. 2 and 3a–c) as is characteristic for *Acropora*, within an open reticulum of connecting skeleton (the coenosteum; e.g. Fig. 3c). Differential growth of the axial and radial corallites creates the ramose growth form and *A. palmata* branches typically grow tangentially to the ocean surface, with the axial corallites primarily responsible for sideways extension. Radial corallites are asymmetrically distributed, with the upward facing sun-lit surface of branches featuring a greater number that are typically more exsert in character, and consequently a lower proportion of the skeleton is coenosteum (Gladfelter, 1977; Gladfelter et al., 1989; also Fig. 2a and c–e).

In *A. palmata*, living tissue remains associated with the perforated framework of skeletal elements for years, allowing further thickening of corallite walls and coenosteum 10 s of cms within the colony (Gladfelter, 1982, 1984). Consequently, porosity decreases with age and distance from the growing tip. Infilling is also uneven perpendicular to axial growth; within the inner areas of the transverse slices, corallite walls and coenosteum demonstrate greater thickening in comparison to outer portions (e.g. Fig. 2c, d, and e). Infilling and corallite density were also slightly higher in the upward, relative to the sediment-facing, skeleton (although this difference was clearer in the larger fossil specimen; see Section 3.1.2). The skeletal surface was covered by a "scale-like" or "shingle" micro-structure (e.g. Fig. 3g and h SEM images), a taxonomic character of Acroporidae (Wallace, 1999). Each of these "shingle" microstructures comprise densely-packed bundles of aragonite fibres (Gautret et al., 2000; Gladfelter, 2007) and represent the surface expression of skeletal infilling (Nothdurft and Webb, 2007 and references therein; Gutner-Hoch et al., 2016). The "shingle" micro-structure pattern was conspicuous in the modern *A. palmata* throughout the coenosteum, between costae (primarily towards the base of corallites), and occasionally within corallites.

Linear extension in *Acropora* occurs through vertical stacking of 'centres of rapid accretion' (CRAs, Stolarski, 2003) from which more fibrous crystal growth emanates. CRA were evident in thin section as a network of dark "threads" and were particularly well-defined along the midline of septa and costae, thinning towards the edge of each structure (Fig. 3b, d, and f). A systematic distribution of CRA was evident, with the highest concentration found within the axial corallite and inner radial corallite walls (Fig. 3b). Otherwise, CRA were rare or absent from the walls

of radial corallites in later ontogenic stages (i.e. with distance from the axial central corallite Fig. 3b and e), and were not visible in the coenosteum or thickening deposits (as is consistent with their mode of formation, e.g. Stolarski, 2003; Gladfelter, 2007; Nothdurft and Webb, 2007).

3.1.2. Fossil A. palmata specimen

In the fossil *A. palmata* a concentrated cluster of primary axial corallites, corresponding to the large size of the colony, was observed across the central axis of the slab and intersected sub-sample 9 (Figs. 2a, 4, and 5d). The prominent CRA visible along the midline of septa and costae in the axial and primary radial corallites of the modern *A. palmata* colony (Fig. 3b, d, f, and g) were also evident in the central axial corallites of the fossil coral (Fig. 5d). Poorly defined CRA were observed in a small number of radial corallites directly adjacent to the axial corallites (Fig. 5b). There were consistent differences in radial corallite density, morphology and direction of growth around the branch slice, equivalent to those observed in the upper- and under-side of the modern specimen and described by Gladfelter (1977) and Gladfelter et al. (1989). These differences were used to orientate the fossil coral (from sediment-facing sub-sample 1, to sub-sample 16 at the upper-facing surface, Fig. 2a). Infilling was higher and porosity lower in the medial region, compared to the outer portions of skeleton. Radial corallites were distributed out from the axial core in all directions, but were more numerous in the top half of the transect (Figs. 4 and 5b). The coenosteum was a clearly defined framework in the lower half of the skeleton (Fig. 5a), whereas it was much less conspicuous in the upper skeleton due to extensive secondary thickening of both coenosteum and (more numerous) corallite walls (see Figs. 4, 5b and c). Consequently, the fossil specimen demonstrated asymmetry perpendicular to axial growth; the infilled (and therefore denser) skeleton characteristic of the central axial region (sub-sample 9) extended into the upper section of the fossil slab (especially sub-samples 10–14), whilst highly porous and permeable skeleton dominated the lower section (sub-samples 1–8) with a sharp transition in density close to the axial corallites in sub-sample 9 (e.g. Fig. 4 arrow and Fig. 5d).

The nature, extent and distribution of diagenetic features are summarised in Fig. 4. Extensive surface dissolution has occurred around the outer edge of the colony, and in the permeable lower skeleton (increasing down towards sub-sample 1) as demonstrated by significant etching of the skeletal surface, loss of the granular microcrystalline surface texture, and exposure of aragonite fibres (Hendy et al., 2007, Fig. 5g). Dissolution had also occurred in the centre of individual trabeculae (defined as "internal dissolution" in Figs. 4, 5a, d, and g) and followed a similar distribution. Evidence of dissolution was either very minor or absent within the denser skeleton (sub-samples 9–15; e.g. Fig. 5b and h). Only the outer surface of the fossil specimen was significantly affected by submarine cements, as is typical of *A. palmata* (Macintyre, 1977; Lighty et al., 1982; Cross and Cross, 1983). Only very minor levels of secondary calcite deposition were evident in thin section (as single spar crystals at rare sporadic points down the transect), except for a discrete 1 mm-wide band of cement along the outer edge of sub-sample 1 (Fig. 5a, e, and f) which was also detected by XRD (~20% of sub-sample 1) and confirmed by Raman microspectroscopy. Minor abiotic aragonite overgrowth (syntaxial acicular crystals) was observed at the margins of scattered pores (e.g. Fig. 5i) becoming less common at the outer edges (Fig. 4).

3.2. Uranium-series geochemistry

*3.2.1. Modern **A. palmata** specimen*

Uranium concentrations ranged from 3.2 to 4.1 ppm ($\bar{x} = 3.6$ ppm) in the 14 sub-samples measured (Fig. 6a, Table EA 1). The [U] were generally lower in the centre (axial corallite and denser infilled material), and increased with distance towards the outer edge (radial corallites and framework).

3.2.2. Fossil A. palmata specimen

Uranium concentration was highest in the central part (e.g. 3.4 ppm in sub-sample 8) and decreased towards both outer edges (~2.5 ppm, Fig. 7a). The outer edges had elevated ^{232}Th concentrations (>1 ppb in sub-samples 1, 2 and 16), but [^{232}Th] was <0.25 ppb for all remaining sub-samples (Fig. 7b). The [^{230}Th/^{238}U]$_{act}$ values were also highest at the edges, and followed a systematic pattern, inverse to [U], with the central sub-sample 9 displaying the lowest value (Fig. 7c, Table EA 2). The lowest δ^{234}U values (~90‰) were also in the central part, which, based on closed-system δ^{234}U evolution from the modern seawater composition (δ^{234}U = ~147‰), would correspond to an age of ~170 ka. The δ^{234}U increased progressively outwards from the central part, reaching a maximum of 120‰, before decreasing in the outermost sub-samples (Fig. 7d). Consequently, the spread in U-series ages, derived by combining the δ^{234}U and [^{230}Th/^{238}U]$_{act}$ values was large; from 159.4 ± 1.1 ka (sub-sample 9) to 503.7 ± 29.2 ka (sub-sample 16), with an infinite age for sub-sample 1 (Fig. 7f).

3.3. Organic geochemistry

*3.3.1. Modern **A. palmata** specimen*

AA leaching was not detected in the isothermal heating experiments, indicating that the *A. palmata* intra-crystalline protein fraction effectively operates as a closed system (Fig. EA 1, Table EA 3). Although values and precision of age-dependent parameters (e.g. % FAA Asx; Fig. 6c, racemisation; Fig. 6d and e, Table EA 1) were low in such recently deposited skeleton, FAA D/L was significantly higher in the oldest skeletal material at the base of the colony. The highest THAA concentrations ([total]) were measured in the central axial corallite of the mid-slice, and the lowest in the tip and thickened base sub-samples (Fig. 6b, Table EA 1). The [Asx] mirrored this result (Fig. EA 2c and d). AA composition was dominated by the acidic amino acids Asx and Glx (Fig. EA 2); a common characteristic of scleractinians (Young, 1971; Mitterer, 1978; Constantz and Weiner, 1988; Cuif et al., 1999; Ingalls et al., 2003; Tomiak, 2013).

3.3.2. Fossil A. palmata specimen

The extent of racemisation and hydrolysis (recorded by % FAA) was considerably higher in the fossil *A. palmata* colony than in the modern sample (Fig. 8b–d, Table EA 4), reflecting a significant time span for intra-crystalline protein degradation to have occurred. Typical of all closed-system biominerals (e.g. Penkman et al., 2008, 2011), the FAA D/L values were higher than the THAA D/L (Fig. 8c–f, Table EA 4), which is attributed to FAA formation via hydrolysis of already highly racemised terminal amino acids. Both Asx and Ala seem to have effectively reached equilibrium, as would be expected, given the relatively rapid racemisation rates of these amino acids (e.g. Goodfriend, 1992; Goodfriend et al., 1992; Collins et al., 1999; Penkman et al., 2011; Hendy et al., 2012). No systematic pattern in racemisation (D/L) was observed across the transect for any AA except THAA Asx (Fig. 8d), for which a slight increase in D/L appeared to occur in the upper section, although variability was relatively high (e.g. sub-samples 9–16, $\bar{x} = 0.825 \pm 0.026$ vs. sub-samples 1–8, $\bar{x} = 0.817 \pm 0.018$ 2 SD).

The skeletal AA composition of the fossil *A. palmata* colony was similar to the modern (Figs. EA 2 and EA 3) and dominated by Asx ($\bar{x}$ THAA = 47.1 ± 2.8% and FAA 54.3 ± 2.2%; 2 SD sub-samples 2–16). With the exception of sub-sample 1, mol% Asx (THAA and FAA) was at its highest in the central skeletal material (Fig. EA 3), as observed in the modern coral. Decomposition of skeletal proteins and component AAs, such as Ser decomposition into Ala (Vallentyne, 1964), caused some differences in composition between the modern and fossil colonies. Decomposition reactions contribute to the observed reduction in [total] relative to the modern colony (compare Figs. 6b and 8a), although sub-samples from the dense upper section of the transect exhibited values closest to the modern specimen (maximum 861 pmol/mg, sub-sample 12). Sub-sample 1, however, had an extreme low value (total THAA concentration 466 pmol/mg; Fig. 8a), and anomalous AA composition, particularly in the THAA fraction, relative to the other transect sub-samples (Fig. EA 3c; Asx and Glx were 13% and 8% lower, Ala was 8% higher). The% free Asx was >100% (Fig. 8b) which, in samples with an already high level of FAA, is caused by enhanced AA decomposition during the preparative hydrolysis for THAA.

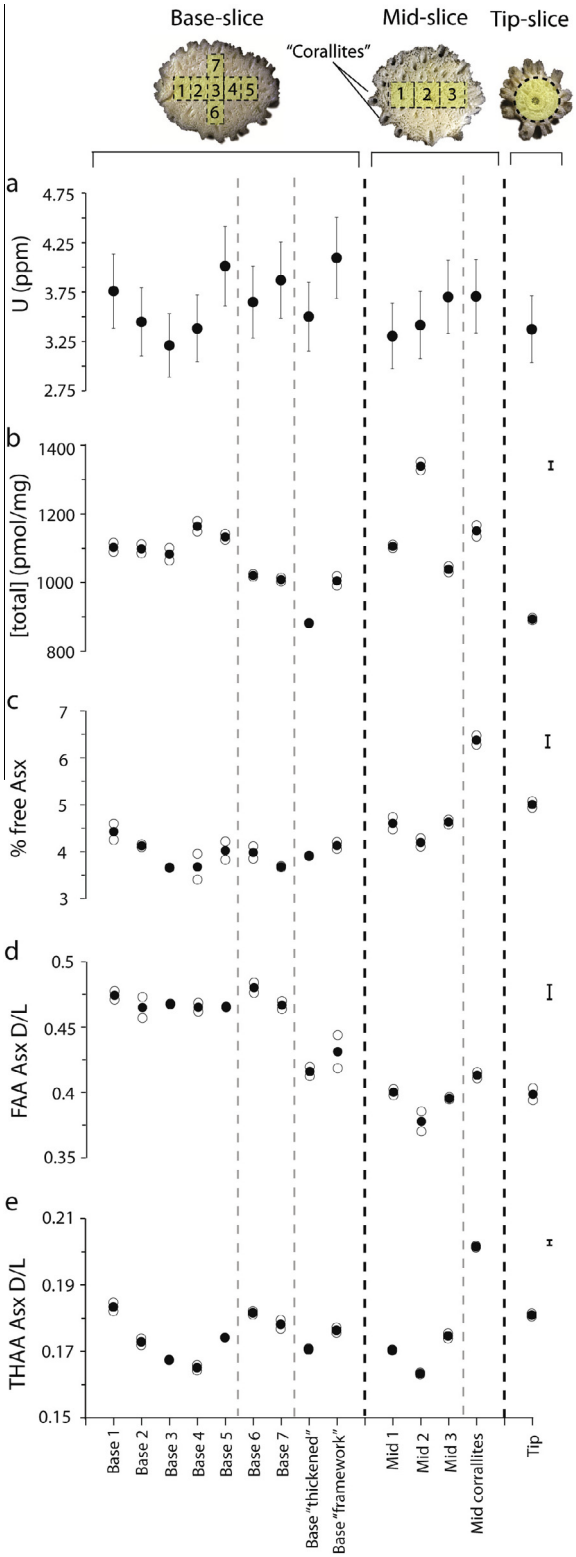

Fig. 6. Geochemical results from the modern *A. palmata* colony. Sub-sample numbers match positions indicated on base, mid and top coral slices (Fig. 1b) with additional samples of "thickened", "framework" and radial "corallites" material. (a) U concentration (ppm) error bars are ±10%, based on repeated U/Ca measurements of a coral sample and environmental factors on the U/Ca ratio (e.g. temperature) within the coral. (b) Total amino acid concentration ([total]), (c) Percentage free Asx (% FAA Asx), (d) racemisation of Asx in the free amino acid fraction (FAA Asx D/L), and (e) racemisation of Asx in the total hydrolysable amino acid fraction (THAA Asx D/L). In (b)–(e), replicate AA measurements (open circles) and mean values (black circle), are shown, along with 95% confidence interval repeatability (CIR) error bars.

4. DISCUSSION

Below, we discuss how the process of skeletogenesis in *A. palmata* influences diagenesis and in turn, amino acid

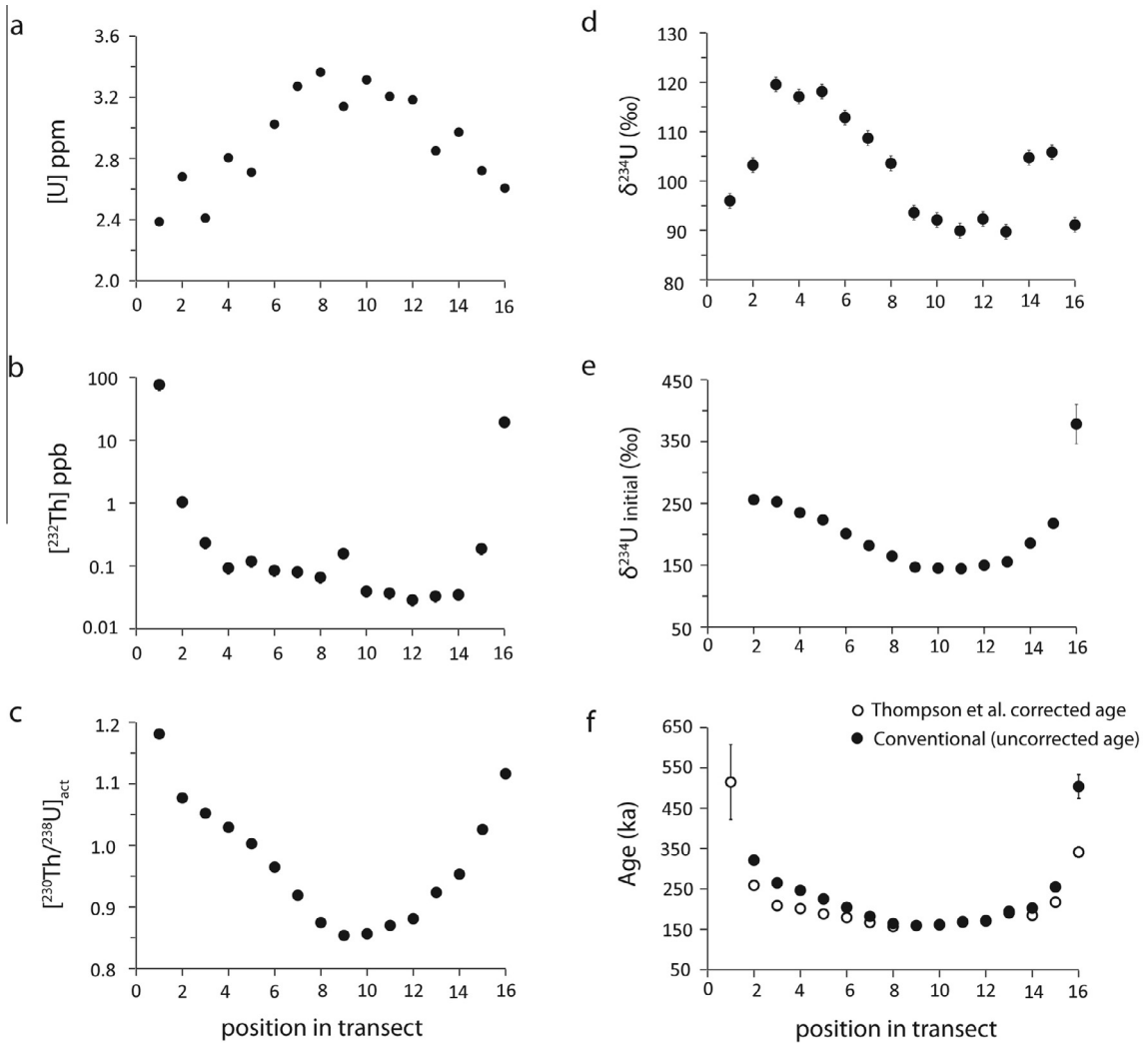

Fig. 7. U-series geochemistry in the fossil *A. palmata* colony. (a) ^{238}U concentration, (b) ^{232}Th concentration (log scale), (c) [$^{230}Th/^{238}U$] activity, (d) $\delta^{234}U$ measured, (e) back-calculated $\delta^{234}U_{initial}$, and (f) U-series ages, uncorrected (conventional; filled circle) and corrected (using Thompson et al., 2003; open circle; note that no conventional U-series age could be obtained for sub-sample 1). For all graphs, plotted error bars as given in Table 1. Error bars not visible are smaller than the marker symbols.

racemisation and U-series geochemical trends, with implications for dating fossil corals. Finally, we discuss the application of the fossil specimen for sea-level reconstruction.

4.1. Skeletal controls on diagenesis in *A. palmata*

The U-series chronometer relies upon closed-system behaviour, so that changes in isotopic ratios are purely a consequence of decay and ingrowth. Similarly, AAR dating assumes that the amino acids have degraded within a closed system in which the products of the reaction are retained and sources of contamination (exogenous amino acids), are excluded. As post-mortem diagenetic changes to coral skeleton can compromise the closed-system, identifying how skeletal morphology controls patterns of diagenesis is key to selection of the most pristine material for dating. The central skeleton is likely to experience reduced exposure to later reactive fluids (marine, phreatic or meteoric) simply as a consequence of the restriction of percolating waters by the surrounding skeleton, but differences in skeletal micro-structure (including skeletal porosity, aragonite fibre texture and packing of fibres) also control the vulnerability of a coral species to skeletal dissolution (Constantz, 1986; Dullo, 1987). In *A. palmata* asymmetric corallite distribution and the extent of secondary thickening *perpendicular* to axial growth creates strong porosity gradients, which in the fossil specimen of *A. palmata* correlate strongly with zonation in secondary diagenetic features (Fig. 4). For example, the porous coenosteum-dominated skeleton exhibited high levels of internal and surface dissolution, as did the outermost upper-facing layer where, despite some evidence of secondary thickening, corallite walls were thinner than deeper into the branch, and

corallite density was relatively low (Fig. 4). Dissolution was either very minor or absent in the central skeleton, particularly in the denser upper zone (sub-samples 9–14).

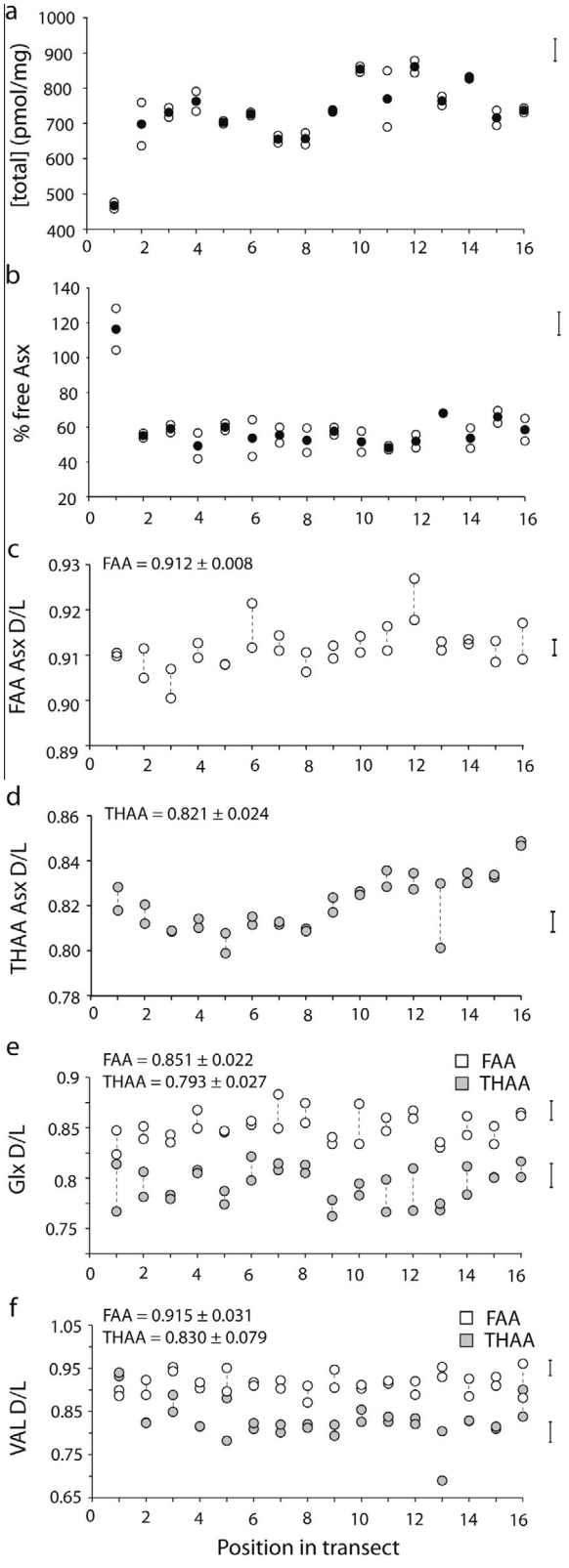

Since CRA are susceptible to dissolution (James, 1974; Bar-Matthews et al., 1993; Gautret et al., 2000; Perrin, 2004; Perrin and Smith, 2007), their preservation within multiple axial corallites of the fossil colony (Fig. 5d) is strong evidence that the very central core of the fossil *A. palmata* branch is in pristine condition.

4.2. Impact of diagenesis on skeletal amino acids in *A. palmata*

Potentially, diagenetic processes of dissolution could affect the organic fraction of a coral skeleton through leaching of intra-crystalline AAs, whereas recrystallisation could incorporate 'foreign' AAs leached from elsewhere in the coral or from exogenous sources. Lower [total] AA concentrations (Fig. 8a) were found in the fossil colony's outer and more porous skeleton where dissolution was also greatest; however the same systematic trend was seen within the modern colony (i.e. the central core had higher AA concentrations; Fig. 6b). Like the fossil colony, the most central skeletal material in the modern *A. palmata* also demonstrates a slightly greater dominance of Asx (Figs. EA 1 and 2). Rather than signifying diagenesis, and dissolution in particular, the AA results instead suggest that skeletal proteins vary between axial and radial corallites, potentially reflecting the role of the organic matrix in the calcification process (e.g. Allemand et al., 1998). Age-related decomposition of skeletal proteins can explain the reduced total and specific AA concentrations (e.g. Asx and Ser; compare Figs. 6b and 8a) in the fossil *A. palmata.* Further, there is no % FAA trend (Fig. 8b) to indicate preferential loss through a leaching process associated with skeletal dissolution, and finally, AA leaching was not induced in the isothermal heating experiments (Fig. EA 1).

In contrast, it is evident that post-depositional recrystallisation and formation of calcite cement severely alters the AA signal. The calcite-containing sub-sample 1 showed increased % FAA Asx and Glx (Fig. 8b), lower [total] (Fig. 8a), and preferential loss of Asx and Glx (also attributed to calcite overgrowth in *A. palmata* by Husseini (1973)) (Fig. EA 3c and d); this combination of observations is best explained by dilution of the skeletal mass by a protein-poor calcite cement that incorporated free AAs into an intra-crystalline site as it precipitated. This divergence from the pristine AA fingerprint could be used to screen potential samples for calcite contamination, prior to U-series or AAR dating.

Fig. 8. Amino Acid concentration and racemisation in the fossil *A. palmata* colony. (a) Total amino acid concentration ([total]), (b) percentage free Asx (% FAA Asx), (c–f) THAA and FAA racemisation (D/L) values for individual Asx (c and d), Glx (e) and Val (f). Error bars are 95% CIR (see Section 2). In (a) and (b) full procedural replicates (open circles) and mean values (black circle) are displayed. In (c)–(e), full procedural replicates are shown for each sub-sample (connected by a dashed line) and the mean and 2 SD of the 16 sub-samples are reported for each AA, for both the FAA and THAA fractions.

4.3. Potential for amino acid racemisation dating in *A. palmata*

The isothermal heating experiments demonstrate that the intra-crystalline fraction in *A. palmata* operates effectively as a closed-system. Once isolated, amino acids in the skeletal protein undergo racemisation, each at a different rate. With time, the extent of racemisation increases, typically following a concave trajectory, until it finally plateaus as the racemisation reaction approaches dynamic equilibrium.

Observations from massive *Porites* sp. show that FAA Asx D/L has greater dating precision than THAA Asx D/L in young Holocene corals (Hendy et al., 2012). In the decadal life-span of the modern *A. palmata* coral, the extent of racemisation of FAA Asx D/L was already consistently greater in material from the base of the colony (i.e. the oldest skeleton) than nearer to the growing tip (Fig. 6d). Furthermore, variability in Asx D/L values perpendicular to growth was lower in the FAA than the THAA fraction (Fig. 6e). In both the modern and fossil *A. palmata* colonies, the highest THAA Asx D/L values were generally associated with skeleton dominated by radial corallites (Figs. 6e and 8d), which may also indicate a specificity of skeletal proteins in the organic matrix of these skeletal structures.

The geochronological potential of AAR in Pleistocene coral was last explored by Husseini (1973) and Wehmiller et al. (1976) and, using ion-exchange chromatography and a mix of species, both studies identified non-concordance between the extent of racemisation of the AA Ile and "known" age. Since this work, studies have shown that racemisation is species-dependent (e.g. Lajoie et al., 1980), and new techniques have been developed to isolate the intra-crystalline fraction, accurately measure FAA racemisation, and analyse multiple AAs (Sykes et al., 1995; Kaufman and Manley, 1998; Penkman et al., 2008; Wehmiller et al., 2012). This progress has reduced uncertainty in AAR-age estimations through selection of AAs best suited to the time range under examination and integration of information from a suite of different AAs (Penkman et al., 2011). In addition, deviation from systematic covariance between different AA, or between the THAA and FAA fraction, can be used to identify compromised samples (e.g. Kaufman, 2006; Penkman et al., 2007; Kosnik and Kaufman, 2008; Tomiak et al., 2013).

Our results demonstrate that Ile, Leu and Phe racemisation (when analysed by RP-HPLC) are not suitable for dating fossil *A. palmata*, due to high analytical variability resulting primarily from low skeletal concentrations. Asx, Glx, Ala, and to a lesser extent Val, all occur at high relative skeletal concentrations (Fig. EA 2) and are sufficiently well resolved by RP-HPLC. The data collected from the fossil specimen (Fig. 8e and f) demonstrates that THAA Glx and Val, and FAA Glx have almost certainly not reached equilibrium; these measures have also been successfully used to discriminate between calcitic biomineral samples of different age at higher D/L values than observed here (Penkman et al., 2011). The results therefore suggest that, for similar diagenetic temperatures to those experienced in Barbados, Glx and Val will prove the most useful AAs for dating mid-Pleistocene *A. palmata*. Further, no systematic pattern in Glx or Val D/L (Fig. 8e and f) was observed between sub-samples from the well-preserved central material and those that have experienced diagenetic alteration through dissolution (internal and/or surface). Minor sporadic calcite precipitation below the detection limit of XRD did not appear to significantly affect D/L, and consequently, AAR dating is possible from coral samples where reliable U-series dates are not obtainable. In contrast, sub-sample 1 demonstrated elevated THAA Val D/L (in addition to the atypical AA composition and concentration) indicating that coral skeleton with significant (in this case ~20%) levels of recrystallisation to calcite is too altered for AAR dating. Further study is required to determine the extent to which calcite cementation influences AAR in coral.

AAR data derived from fossil coral will primarily be useful for relative dating techniques, using D/L values from skeletal samples of the same species derived from geographic regions that share an equivalent temperature history (as racemisation is temperature dependent; e.g. Bada, 1972; Brooks et al., 1990; Miller et al., 1992; Wehmiller and Miller, 2000; Kaufman, 2000, 2006). Relative dating does not require assumptions regarding the complex mechanisms and kinetics underlying racemisation. Using racemisation to acquire absolute ages for fossil *A. palmata* would be a more complex and data-heavy undertaking because it would involve a hybrid approach in which independently dated samples constrain racemisation reaction kinetics established from isothermal heating of modern samples. This process has been used to acquire absolute dates for a variety of biominerals (e.g. Kaufman, 2000) although not for coral, for which extrapolating reaction kinetics from high-temperature experiments is not a valid technique (Tomiak et al., 2013). Deriving an absolute date from the AAR data collected here was therefore not attempted. However, preliminary results demonstrate strong concordance between U-series age (~80 and >200 ka) and D/L (Glx and Val) in *A. palmata*, and suggest that AAR has considerable promise for age estimation of Pleistocene corals (Hodge, 2011).

4.4. Screening techniques and open-system models for obtaining reliable U-series age determinations

Considering the Pleistocene age of the fossil *A. palmata*, the extent of skeletal diagenesis is relatively minor. In spite of this, the derived U-series ages vary by 344 ky, or 162 ky when outer edge sub-samples 1 and 16 are excluded (Fig. 7f, Table 1). This confirms that physical preservation alone, such as minor secondary aragonite and calcite overgrowth (see Section 3.1.2 and Fig. 4) cannot reliably identify U-series open-system behaviour (e.g. Hamelin et al., 1991; Bar-Matthews et al., 1993; Stirling et al., 1998; Scholz et al., 2007) and necessitates the application of "post-analytical" screening methods (e.g. Stirling and Andersen, 2009). One such method is screening for anomalous [U] (e.g. Hamelin et al., 1991; Thompson et al., 2003), but the appropriate [U] range is difficult to establish because

Table 1
U-series isotopic measurements of the fossil *A. palmata* colony.

Cross-section position	^{238}U[a] (ppm)	±2 SD	^{232}Th [b] (ppb)	±	$\delta^{234}U_{meas}$[c] (‰)	±2 SD	$\delta\ ^{234}U_{initial}$[d] (‰)	±2 SD	$(^{230}Th/^{238}U)_{act}$[e]	±2 SD	Conventional age (ka)[f]	±2 SD	Corrected age (ka)[g]	±2 SD
1	2.39	0.01	76.72	15.34	96.0	1.5			1.181	0.003			514.78	93.0
2	2.68	0.01	1.04	0.21	103.2	1.5	256.0	5.6	1.077	0.003	321.38	5.72	259.04	6.21
3	2.41	0.01	0.23	0.05	119.5	1.5	252.7	4.0	1.052	0.003	264.91	3.30	208.81	10.81
4	2.80	0.01	0.09	0.02	117.1	1.5	235.1	3.5	1.029	0.003	246.65	2.76	201.45	7.74
5	2.71	0.01	0.12	0.02	118.1	1.5	223.3	3.2	1.003	0.003	225.36	2.23	188.16	5.20
6	3.02	0.02	0.08	0.02	112.9	1.5	201.2	2.9	0.965	0.003	204.50	1.80	179.27	2.72
7	3.27	0.02	0.08	0.02	108.7	1.5	181.8	2.6	0.919	0.002	182.12	1.42	166.83	1.35
8	3.36	0.02	0.07	0.01	103.6	1.5	164.7	2.4	0.875	0.002	164.22	1.16	156.82	1.12
9	3.14	0.02	0.16	0.03	93.6	1.5	146.9	2.4	0.854	0.002	159.39	1.10	159.45	1.72
10	3.31	0.02	0.04	0.01	92.1	1.5	145.2	2.4	0.856	0.002	161.03	1.12	161.78	1.90
11	3.21	0.02	0.04	0.01	89.9	1.5	144.5	2.5	0.870	0.002	167.80	1.22	168.88	2.07
12	3.18	0.02	0.03	0.01	92.3	1.5	150.0	2.5	0.881	0.002	171.70	1.27	170.42	1.72
13	2.85	0.01	0.03	0.01	89.7	1.5	155.5	2.7	0.924	0.002	194.53	1.64	190.57	2.04
14	2.97	0.01	0.03	0.01	104.7	1.5	185.8	2.8	0.953	0.003	202.76	1.78	184.58	2.26
15	2.72	0.01	0.19	0.04	105.8	1.5	217.7	3.6	1.026	0.003	255.16	3.03	217.33	7.08
16	2.61	0.01	19.44	3.89	91.1	1.5	378.4	31.9	1.116	0.003	503.73	29.25	341.27	12.49

[a] Uranium concentration (^{238}U) was determined from the measured $^{238}U/^{233}U$ and the known ^{233}U concentration of the spike. For U concentration measurements, the sample weighing processes is the major contributor of error; here we use a conservative error estimate of ±0.5% of the [^{238}U] value, in line with previous studies (e.g. Andersen et al., 2007, 2008).

[b] ^{232}Th concentration was determined using the measured ($^{230}Th/^{232}Th$) in order to identify detrital (non-radiogenic) thorium contamination. Only sub-samples 1, 2, and 16 demonstrated significant ^{232}Th; the other pieces all recorded <5 mV on the Faraday cup and therefore the error in these measurements is dominated by the large uncertainties in the measured ^{232}Th during the analytical session. Error was conservatively estimated as 20% of the [^{232}Th] value following (Andersen et al., 2010a).

[c,d] The $\delta^{234}U$ was derived using Eq. (1) and the $\delta^{234}U_{initial}$ was derived using the samples $\delta^{234}U$ and its U-series age, by rearrangement of $\delta^{234}U_{measured} = (\delta^{234}U_{initial})e^{-\lambda_{234}t}$, where λ_{234} = decay constant for ^{234}U and t = time. Errors shown for $\delta^{234}U$ values (±1.5‰, 2 SD) represent the long-term reproducibility of HU-1, CZ-1 and seawater standards (see Andersen et al., 2013).

[e] Errors shown for $[^{230}Th/^{238}U]_{act}$ are based on integrated reproducibility of the TEDDii $^{230}Th/^{229}Th$ ratio which was run every 3 unknowns during the analyses, and reproducibility of in-house $^{233}U/^{238}U$ standards (see Andersen et al., 2013), giving a combined total ±2.7‰ (2 SD) uncertainty of the measured $[^{230}Th/^{238}U]_{act}$. The reproducibility of the full-procedural (matrix-matched) coral standards, validates the use of these average uncertainty estimates.

[f] U-series ages (ka) were calculated iteratively (using Microsoft Solver), using the decay constants of Cheng et al. (2000) and spike calibration based on secular equilibrium standards in Andersen et al. (2008). The uncertainty in the U-series age includes the analytical error contribution from the parameters $\delta^{234}U$ and $[^{230}Th/^{238}U]_{act}$. Decay constant uncertainties are not incorporated (their contribution to error is minor for coral of this age; e.g. Andersen et al., 2010a).

[g] The corrected ages were calculated by applying the Thompson et al. (2003) open-system model, using the present-day seawater $\delta^{234}U = 147‰$ (Andersen et al., 2010b). The Thompson open system model equations are described in detail in Thompson et al. (2003) and the iterative calculation process were performed in a Microsoft Office Excel spreadsheet kindly provided by Dr. W. Thompson. Errors for the corrected ages were determined as detailed in Thompson et al. (2003).

primary [U] variation exists between and within individual colonies (e.g. Schroeder et al., 1970; Robinson et al., 2006; Shirai et al., 2008), as seen in the modern *A. palmata* (lower [U] in the centre increasing towards the outer edge; Fig. 6a). Since [U] has been documented to vary on micro-structural scales, including across individual septa in acroporids (e.g. Schroeder et al., 1970; Shirai et al., 2008), changes in the proportion of corallites, coenosteum and extent of infilling are likely to explain colony trends and differences, together with the temperature control on U incorporation into aragonite (Min et al., 1995). Although [U] in the fossil *A. palmata* varies over a similar magnitude of values to the modern specimen, the trend is effectively antiphase, with the highest [U] in the centre. Screening using a typical [U] range of 2.64–3.84 ppm for *A. palmata* (Thompson et al., 2003; Scholz and Mangini, 2007) would only exclude sub-samples 1, 3 and 16 (leaving a derived age range of 162 ky). Screening for high quantities of ^{232}Th (e.g. >1 ppb), which is assumed to be inherited post-mortem from detrital material that also contains extraneous ^{230}Th, ^{234}U, ^{235}U and ^{238}U, has also been employed to identify compromised samples (e.g. Stirling et al., 1998; Thompson et al., 2011). Here however, ^{232}Th screening would only exclude the 3 outermost sub-samples and lower the derived age range within the single colony to 105 ky.

The most critical "post-analytical" screening method is to verify closed-system evolution by comparing the back-calculated δ^{234}U ($\delta^{234}U_i$; the initial δ^{234}U value of the skeleton when precipitated; Fig. 7e) to the modern δ^{234}U seawater composition of 147‰, assuming this value has stayed relatively constant since the mid-Pleistocene (e.g. Edwards et al., 1987; Hamelin et al., 1991; Gallup et al., 1994; Stirling and Andersen, 2009; Andersen et al., 2010a). This powerful method has been reliably used to detect samples demonstrating significant open-system behaviour and to constrain U-series age uncertainties (e.g. Gallup et al., 1994; Stirling et al., 1995, 1998). However, the technique fails to consistently identify *all* compromised samples, such as those demonstrating subtle open-system behaviour (e.g. Scholz and Mangini, 2007). The method is also limited by underlying assumptions regarding the seawater δ^{234}U composition over time; for instance, there is increasing evidence for a 5–10‰ lower δ^{234}U during parts of the last glacial period (e.g. Esat and Yokoyama, 2006; Thompson et al., 2011) compromising the use of a fixed δ^{234}U composition based on modern seawater (e.g. Stirling and Andersen, 2009). Irrespective of these limitations, the $\delta^{234}U_i$ screening criteria have significantly improved the reliability of U-series dates, particularly when used in combination with other screening methods (such as [U] and [Th] and calcite content).

However, the limitations of these screening techniques and the necessity to reject a large number of samples due to open-system behaviour has led to the development of approaches that use apparent systematics in the U-series geochemistry to extract reliable ages. Significantly, similar aged corals within the same reef formation often display a positive correlation between δ^{234}U and $[^{230}Th/^{238}U]_{act}$ (e.g. Gallup et al., 1994; Stirling et al., 1998; Thompson et al., 2003; Villemant and Feuillet, 2003; Potter et al., 2004). Building on earlier work (Gallup et al., 1994; Fruijtier et al., 2000; Henderson and Slowey, 2000), Thompson et al. (2003) devised an alpha-recoil model coupling addition/loss of the daughters ^{234}U and ^{230}Th. In this model, differential equations constrain "addition lines" on a δ^{234}U vs. $[^{230}Th/^{238}U]_{act}$ plot, that extend away from

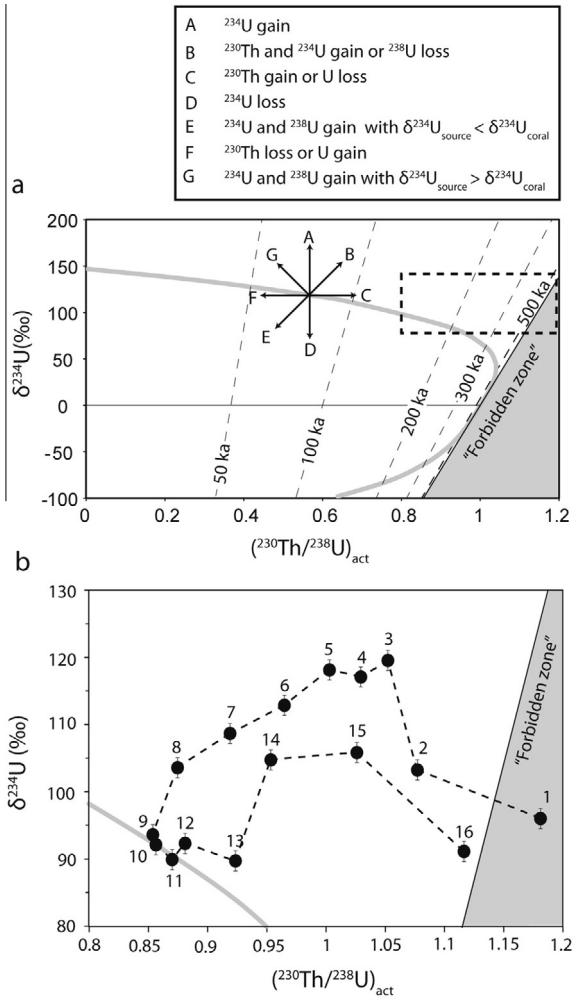

Fig. 9. (a) Graphic of δ^{234}U vs. $[^{230}Th/^{238}U]_{act}$ (modified from Scholz et al., 2007). The seawater evolution curve (thick grey line) tracks a sample decaying within a closed-system over time, that has evolved from an initial δ^{234}U equal to that of modern seawater (147‰). Closed-system isochrons (dashed grey lines) are shown. Samples with isotopic ratios plotting in the "Forbidden zone" are unattainable under closed-system radioactive decay. Labelled arrows (black) illustrate the potential effects of various processes on the isotopic composition of the coral skeleton. The effect of these processes will strongly depend upon timing (relative to skeletal formation), duration magnitude, and the occurrence of contemporary processes (Scholz et al., 2007); they can result in apparent ages both younger and older than the true. (b) Plot of measured δ^{234}U vs. $[^{230}Th/^{238}U]_{act}$ in the fossil *A. palmata* coral. Individual points are numbered according to their respective sub-sample on the fossil transect (Fig. 2a) and are connected with a black dashed line. The position of the data points plotted in (b) is indicated in (a) by the (dashed outline) box. Error bars are smaller than the marker symbols.

the closed-system evolution, whilst anchored by the modern seawater $\delta^{234}U$ composition. This open-system age model does not account for any bulk U loss or addition, as observed in this fossil coral. Other studies have used linear regression to model the observed relationship between $\delta^{234}U$ and $[^{230}Th/^{238}U]_{act}$ of a suite of similar aged-samples and derived an open-system age from the intersection point between the regression line and a seawater evolution curve (e.g. Scholz et al., 2004; Potter et al., 2004). The spread in the $\delta^{234}U$ and $[^{230}Th/^{238}U]_{act}$ compositions of the fossil *A. palmata* in this study demonstrates that this method would also be of limited use in obtaining robust ages (e.g. see Fig. 9b). As shown with the U-series results for the fossil *A. palmata* sample, all open-system models have recognised limitations (Scholz and Mangini, 2007; Scholz et al., 2007; Stirling and Andersen, 2009; Obert et al., 2016) and models are typically employed without the exploration of links between U-series geochemistry and the distribution of micro-structural or diagenetic textures.

4.5. Linking *A. palmata* skeletal structure and diagenesis to open-system U-series geochemistry

The fossil *A. palmata* transect displays considerable and systematic variability in U-series geochemistry (Fig. 7). However, under close scrutiny, it is evident that the patterns in U-series data can be directly linked to the skeletal structure and diagenetic features, providing an opportunity to explore the mechanistic processes behind these observations and the timing of diagenetic changes. The outermost skeleton shows the highest degree of dissolution, calcite content and $[^{232}Th]$. The highest rates of water through-flow would have occurred in this part of the colony, and in addition, upon death, this surface tissue zone would have been exposed to a layer of decaying organics, which would have readily complexed external Th and U (e.g. Chabaux et al., 2003 and see elevated ^{232}Th in Fig. 7b). Unsurprisingly, the outer sub-samples exhibit very discordant U-series compositions (sub-samples 1, 2 and 16; Fig. 9b) and unreliable U-series age estimates (Table 1).

Post-depositional diagenesis has also caused systematic variability in [U] further into the skeleton (Fig. 7a). Although both the modern and fossil coral will have different primary [U] because integrated skeletal material was deposited across a range of SST values and then further infilled over periods of years to decades, the trend in [U] in the fossil skeleton clearly differs and is, if anything, in anti-phase to the modern specimen, strongly suggesting that this variability is of diagenetic origin. However, only minor deviation from closed-system behaviour is indicated for the central core region, which plots on (or very close to) the seawater evolution curve in the $\delta^{234}U$ vs. $[^{230}Th/^{238}U]_{act}$ space (sub-samples 9–12; Fig. 9). Visual evidence such as minimal dissolution and well-preserved CRA also indicate that this central zone experienced the least alteration, and likely represents the primary [U] of the fossil coral skeleton. This implies U-loss increasing outwards (Fig. 7a), whilst the absence of significant calcite indicates that recrystallisation is not a pre-requisite for this significant U loss. Similarly, the lack of any distribution trend in the sporadic low levels of secondary aragonite (Fig. 4) suggests that it also is not the primary cause of systematic patterns in [U] or $\delta^{234}U$ (contrary to e.g. Gvirtzman et al., 1973; Lazar et al., 2004).

The positive correlation between $\delta^{234}U$ and $[^{230}Th/^{238}U]_{act}$ seen within the single fossil colony at the mm-scale (Fig. 9b; excluding the outermost sub-samples 1, 2 and 16) mimics previous observations at the 10 s of metres scale across sections of fossil coral reef (e.g. Gallup et al., 1994; Stirling et al., 1998; Thompson et al., 2003; Villemant and Feuillet, 2003; Potter et al., 2004; Scholz et al., 2004). This relationship indicates ^{230}Th–^{234}U gain, and/or ^{238}U loss (arrows B or C in Fig. 9a) is spatially systematic, with progressive deviation away from the seawater evolution curve with increasing proximity to the edge of the slice (Fig. 9b). We suggest that two processes may together account for these trends in U-series geochemistry (Figs. 7a, c, d, and 9b):

1. *Uranium loss from dissolution*. The more central areas of the skeleton are exposed to lower levels of percolating meteoritic fluids and consequently dissolution is greatest towards the outer part of the coral skeleton (Fig. 4), resulting in a progressive increase in bulk U leaching from the crystal lattice (Fig. 7a). Given the observed distribution of the two dissolutional processes (Fig. 4) and that the upper skeletal sub-samples (13–16) also demonstrate a high degree of U loss (Fig. 7a), one can speculate that internal dissolution (occurring within the centre of individual trabecular; Figs. 4 and 5), rather than surface dissolution primarily controls this process. Thorium, being less soluble, is not influenced, resulting in higher $[^{230}Th/^{238}U]_{act}$ towards the outer part of the transect (Fig. 7c).
2. *U-series daughter addition*. Alpha-recoil processes occurring in an external source could have mobilised ^{234}Th (which decays to ^{234}U) via an aqueous intermediate, which subsequently, could have been absorbed onto the analysed coral skeleton, thereby increasing the $^{234}U/^{238}U$ (e.g. Fruijtier et al., 2000; Thompson et al., 2003). The spatially systematic pattern observed in $\delta^{234}U$ could arise if skeletal absorption of U did not occur uniformly; ^{234}U addition would be promoted in those outer, more porous, areas of skeleton (here, sub-samples 3–8, 14–15) that experienced higher through-flow of reactive fluids, and possess a larger surface area, increased by surface and/or internal dissolution, for absorption (Figs. 4 and 5). The addition of ^{230}Th may also have occurred via the same processes responsible for the ^{234}Th mobility and adsorption (Thompson et al., 2003; Villemant and Feuillet, 2003) and so contribute to the observed positive systematic pattern of $\delta^{234}U$ vs. $[^{230}Th/^{238}U]_{act}$ (Fig. 9b).

The mechanisms proposed here emphasise through-flow of meteoric waters in causing spatial variability in U-series geochemistry within coeval sub-samples of a single specimen. Only a limited number of studies have used multiple sub-samples within individual colonies to explore the impact of diagenesis on U-series systematics (e.g. Scholz et al., 2004,

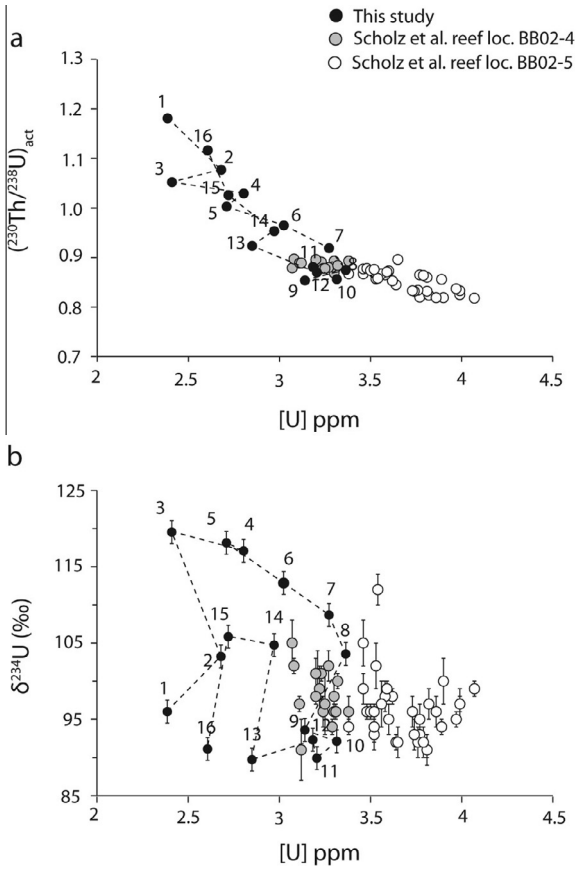

Fig. 10. Pleistocene Barbados *A. palmata* U-series geochemistry (a) $[^{230}Th/^{238}U]_{act}$ vs. ^{238}U concentration, and (b) $\delta^{234}U$ vs. ^{238}U concentration. The position of each sub-sample within the fossil transect is indicated next to the data-point (black circle); plotted error bars as given in Table 1. Data from *A. palmata* at two closely positions reef locations in Barbados (Scholz et al., 2007; white and grey circles) is also shown. Scholz et al. (2007) proposed that sub-samples at location BB02-5 had gained/lost mobilised U, whilst those at BBO2-4 did not demonstrate this open-system behaviour. Error bars for $\delta^{234}U$ and $[^{230}Th/^{238}U]_{act}$ are based on the uncertainty reported by Scholz et al. (2007), though as no uncertainty was reported for U concentration, the same uncertainty was used as was applied here. Error bars not visible are smaller than the marker symbols.

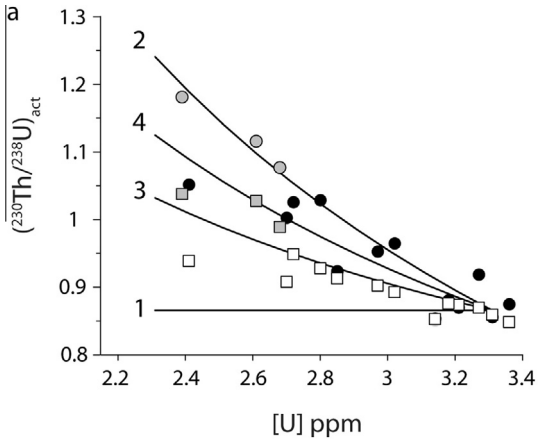

Fig. 11. Diagenesis trends in $[^{230}Th/^{238}U]_{act}$ vs. U concentration (ppm). Data derived from the fossil *A. palmata* colony are represented by circles. Four U-loss scenarios (lines 1–4), have been modelled; for each it is assumed that the $\delta^{234}U_i$ of the colony was equal to modern seawater (147‰) and the primary U concentration was that measured in sub-sample 10 (3.31 ppm). If leaching occurred shortly after skeletal formation then the effect on the measured $[^{230}Th/^{238}U]_{act}$ will be negligible (line 1), whereas recent U loss would have a significant effect on $[^{230}Th/^{238}U]_{act}$ (line 2). U loss occurring during MIS 5.5–5.3 (~120 ka) would provide an intermediate trajectory between these two end-members (line 3). Alternatively leaching of U could be continuous, rather than episodic (line 4). In an attempt to isolate the impact of U leaching from open-system Th-daughter addition, the $[^{230}Th/^{238}U]_{act}$ was re-calculated for each sub-sample using the Thompson et al. (2003) open-system model (square symbols; see main text for details). The outer sub-samples 1, 2 and 16, which exhibited higher ^{232}Th, are marked in grey.

2007; Andersen et al., 2010a; Thompson et al., 2011; Obert et al., 2016). Scholz et al. (2007) reported U-series results on sub-samples of three separate similar-aged *A. palmata* colonies also from Barbados (location BB02-5, Cave Hill; Fig. 1), but in this case including corals that had *gained* [U] (negative correlation between [U] and $[^{230}Th/^{238}U]_{act}$ in Fig. 10a; [U] > 3.24 ppm typical of *A. palmata*; Cross and Cross, 1983). Our fossil *A. palmata* appears to form a "counterpart" to the corals of Scholz et al. (2007) by expressing the same relationship between [U] and $[^{230}Th/^{238}U]_{act}$, but with net U *loss* (Fig. 10a). The sub-samples maintaining their primary [U] signal (9–12) overlie values from the "undisturbed" Scholz et al. colony (Fig. 10).

Assuming U loss was the major open-system process to have operated in this fossil coral, then the timing at which the loss occurred will impact the observed $[^{230}Th/^{238}U]_{act}$. Uranium loss occurring shortly after skeletal formation will have a negligible impact on $[^{230}Th/^{238}U]_{act}$, whilst recent U loss will have the most significant effect. The data from the fossil *A. palmata* appears to correspond best with a recent U loss scenario (it lies closest to the trajectory of line 2 in Fig. 11). However, application of the Thompson et al. (2003) model reduces the variability in U-series age estimates to some extent (Fig. 7f), which, when combined with the patterns in U-series geochemistry, indicates that U-series daughter addition must also have occurred. Each sub-sample can be corrected for daughter-addition using the Thompson et al. (2003) model; a corrected $[^{230}Th/^{238}U]_{act}$ composition for each sub-sample can be calculated from the obtained open-system age and the corresponding $[^{230}Th/^{238}U]_{act}$ on the closed-system seawater ^{230}Th-^{234}U-^{238}U evolution curve (Table EA 2). For all sub-samples (Fig. 11), this corrected $[^{230}Th/^{238}U]_{act}$ composition is lower than the equivalent conventional value, and approximates the effect on $[^{230}Th/^{238}U]_{act}$ of the U loss process alone. This corrected $[^{230}Th/^{238}U]_{act}$ data is more consistent with a scenario of later episodic U leaching (line 3 in Fig. 11), for instance, across the MIS 5.5–5.3 sea-level fluctuations (~120–100 ka), when lowering of the sea-level would have exposed the coral reefs to the phreatic zone.

U-series systematics (Fig. 9b) and diagenetic evidence suggests that sub-samples 9–12 of the fossil *A. palmata*

provide the most robust age estimate for the specimen, demonstrating the least sign of open-system behaviour; a primary [U], low [^{232}Th], and minimal evidence of dissolution or secondary overgrowths. The conventional U-series ages for these four dense central sub-samples are 159 ± 1, 161 ± 1, 168 ± 1 and 172 ± 1 ka (Table 1). These ages do not overlap suggesting some minor scale open-system behaviour or potentially minor contamination added during the crushing stage of the sub-samples, but it is not possible to distinguish between these four sub-samples in terms of one being more pristine than another. Instead, further investigation of small scale open-system heterogeneity is required, targeting uncrushed samples at higher resolution over this central part of the transect. Taking this uncertainty into account, we suggest a best U-series age estimate of 165 ± 8 ka (mean age ± the maximum range of the four individual dates). Applying the previously reported criterion of $\delta^{234}U_i = 147 \pm 4‰$ (e.g. Stirling et al., 1995) retains the exact same set of sub-samples. Whilst acknowledging the limitations of using $\delta^{234}U_i$ to detect open-system behaviour (as also discussed in Section 4.3), this study, like others before (e.g. Stirling et al., 1995, 1998) has demonstrated the effectiveness of using $\delta^{234}U_i$ screening in concert with other screening criteria to identify the most reliable ages. That the presumed most pristine coral sub-samples have a $\delta^{234}U_i$ similar to modern seawater, a feature also observed for MIS 7 fossil corals (Gallup et al., 2002; Thompson et al., 2003; Andersen et al., 2010a), could indicate that seawater $\delta^{234}U$ may have been close to the modern composition around 160–240 ka.

4.6. Global implications: Barbados as an MIS 6.5 reef location

The island of Barbados has been rising for at least the past million years (Schellmann and Radtke, 2004b and references therein) preserving a sequence of raised coral reef terraces that have been exploited to document Late Quaternary sea-level change (e.g. Broecker et al., 1968; Bard et al., 1990; Gallup et al., 1994; Potter et al., 2004). The spatial distribution of similarly-aged reefs on Barbados is valuable for differentiating uplift rates across the island, thereby improving reconstructions of past sea-level elevation. The fossil *A. palmata* in our study is from Foul Bay (Fig. 1). The best U-series age estimate of the colony is 165 ± 8 ka (Section 4.5; $n = 4$ sub-samples), close to the ESR dates of *A. palmata* colonies from the Foul Bay reef terraces (~182 ± 18–232 ± 27 ka) when uncertainties in the accuracy of these older ESR ages are considered (Schellmann and Radtke, 2004a). Furthermore, at Salt Cave Point, less than 5 km east of Foul Bay (Fig. 1), a reef section occurs with similar ESR dates (from 191 ± 20 to 215 ± 19 ka) and a single *A. palmata* from 4 m above sea level (msl) yielded a similar conventional U-series age of 168 ± 2 ka ($\delta^{234}U_i = 154 \pm 4$, [U] = 3.26 ppm; Potter et al., 2004). In addition, the U-series age of the Foul Bay sample is similar to U-series ages from an *A. palmata* reef section at ~+36 msl in the Cave Hill transect (Fig. 1) on the western side of Barbados (Gallup et al., 2002; Speed and Cheng, 2004; Scholz et al., 2007), which has an estimated U-series age of 171 ± 7 ka (mean ± conventional age range for the 4 reliably-dated coral samples using a $\delta^{234}U_i$ similar to modern seawater, in Scholz et al., 2007). The overlapping ages for these three units suggests that they were all formed during the MIS 6.5 interstadial.

Estimated linear uplift rates at the western sided Cave Hill transect range from 0.44 to 0.53 m/ka, based on the current elevation of the prolific MIS 5.5 reef relative to the assumed global sea-level at that time (Gallup et al., 2002; Speed and Cheng, 2004; Potter et al., 2004; Thompson and Goldstein, 2005; Scholz et al., 2007). The uplift rate at Foul Bay cannot be estimated in this way, as no MIS 5 reef transects are exposed (Schellmann and Radtke, 2004b). However, both Salt Cave Point and Cave Hill have well-dated MIS 5.3 reef units (Potter et al., 2004) enabling cross-correlation of uplift rates. Based on an estimated constant linear uplift rate of 0.45 ± 0.03 m/ka calculated from the MIS 5.5 Cave Hill section, Potter et al. (2004) estimated the MIS 5.3 sea-level (at 101 ka) to be −14 ± 4 m compared to mean sea level (msl). Assuming the same initial sea-level (−14 ± 4 msl), the MIS 5.3 reef at Salt Cave Point, now with a maximum current elevation of +13 msl and an assumed age of 101 ka (Potter et al., 2004), provides an estimated constant linear uplift rate of +0.27 ± 0.01 m/ka. These uplift rates for Cave Hill (+0.45 ± 0.03 m/ka) and Salt Cave Point/Foul Bay (+0.27 ± 0.01 m/ka) may then be used to approximate the MIS 6.5 sea-level at each locality. Applying the same uplift rates to the MIS 6.5 reef sequence at Cave Hill (presently +36 msl and 171 ± 7 ka; Scholz et al., 2007), the MIS 6.5 sea-level is calculated to be −41 ± 8 msl, similar to earlier published estimates (e.g. Gallup et al., 2002; Speed and Cheng, 2004; Thompson and Goldstein, 2005; Scholz et al., 2007). The MIS 6.5 sea level at Salt Cave Point was based on the fossil coral dated to 168 ± 5 ka (with the error expanded to compensate for the slightly elevated $\delta^{234}U_i$; Potter et al., 2004), and yields an estimate of −41 ± 2 msl (Fig. 12). The *A. palmata* at Foul Bay (+10 msl and 165 ± 8 ka) provides a MIS 6.5 sea-level estimate of −35 ± 7 msl (Fig. 12).

These estimates of relative sea-level from different sites on Barbados during MIS 6.5 are within error of each other (Fig. 12). The Red Sea $\delta^{18}O$ sea-level reconstruction (Grant et al., 2014) suggests that sea-level reached a maximum of ~50 m below mean sea level during MIS 6.5 (Fig. 12). When considering the potential effect of glacio–hydro-isostatic adjustment (vertical displacement caused by the redistribution of ice and melt-water loading during glacial advances and retreats) on Barbados during this period, this is in good agreement with the relative coral-based MIS 6.5 Barbados sea-level estimates. For instance, it is possible that the relative sea-level at Barbados was ~10 m higher than eustatic (meaning "global" sea-level, reflecting the relative volume of water stored in the oceanic basins and ice as opposed to vertical movements of the land) sea-level, similar to that estimated at MIS 5.1 (Potter and Lambeck, 2004). These results show that analysis of additional coral specimens at Barbados localities with exposed MIS 6.5 reef terraces could further refine estimates of MIS 6.5 sea-level at Barbados and provide information on global sea level,

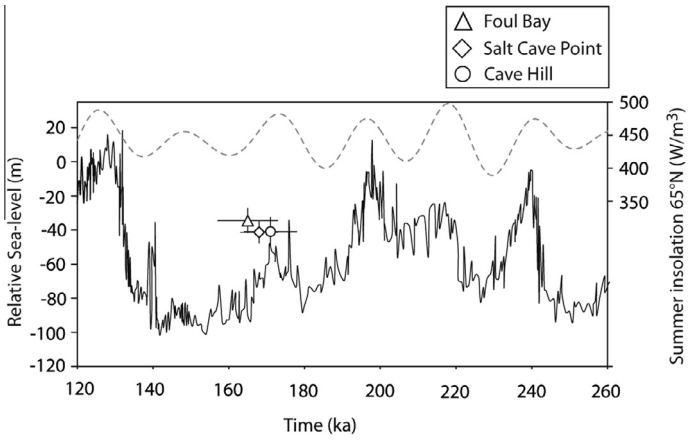

Fig. 12. (a) Global sea-level curve (black solid line; Grant et al., 2014), with the estimated initial sea-level at three locations in Barbados (see main text for calculations). Grey dashed line represents the summer insolation curve (Berger, 1978).

uplift rates on Barbados, and the potential isostatic fingerprinting of source regions of ice melting (Clark et al., 2002).

5. CONCLUSIONS

A. palmata is a major component of Quaternary fossil reefs in the Caribbean and is commonly used for sea-level reconstructions, but its characteristic skeletal architecture, including the asymmetric distribution of corallites and secondary thickening, creates spatial variability in porosity with consequences for geochemical dating approaches. For this reason, conventional U-series ages for *A. palmata* from fossil coral reefs in the Caribbean region are often considered unreliable and therefore unsuitable for the purpose of sea-level reconstruction. We suggest that this micro-structural variability in *A. palmata* controls through-flow of percolating waters, causing spatial heterogeneity in diagenetic alteration and that U-series geochemistry is particularly sensitive to these dissolution processes, in addition to secondary cement formation. Combining our observations with those of Scholz et al. (2007), we suggest that U loss/gain and U-series daughter addition are critical components of the diagenetic evolution and open-system U-series behaviour in *A. palmata*, and no pre-existing "open-system models" (e.g. Thompson et al., 2003) incorporate this combination of diagenetic mechanisms to yield robust age estimates.

Previous studies of *A. palmata* are based on analyses of bulk samples that have not attempted to target the least-diagenetically altered (including dissolution impacted) areas of skeleton for analyses. Our recommendations to improve the reliability of U-series ages and of this valuable sea-level indicator species reduce the number of compromised samples that are analysed include:

- That targeted sampling of an *A. palmata* colony must avoid areas of high porosity, especially the outer surface of colonies and tips, which are vulnerable to dissolution. Instead sampling should focus on the central axial corallite zone and upper side of branches where the density of corallites and the degree of secondary skeletal thickening is highest. Whilst this study focused on samples of *A. palmata*, it is likely that selective sampling of other coral species characterised by regions of denser and more porous skeleton such as faviidae species, would also improve the reliability of subsequent U-series analyses.
- Use of thin sections and SEM to identify the most suitable skeletal material, particularly screening out material showing evidence of internal and surface dissolution. Analysis could also be supplemented with laser ablation (LA) MC-ICPMS to investigate open-system U-series behaviour at a finer scale (e.g. Potter et al., 2005b; Eggins et al., 2005; Spooner et al., 2016).
- U concentration is an important indicator of diagenetic alteration. However, rather than simply applying an "approved" concentration range derived from modern coral, detection of relatively subtle [U] gain or loss processes requires that [U] is measured in multiple sub-samples across the same coral colony.
- Use of amino acid analysis, particularly % FAA and intra-crystalline AAR of glutamic acid and valine in Pleistocene coral as a dating tool in those samples where U-series measurements are compromised by surface and internal dissolution. Given that AA analyses are comparatively time and cost effective relative to U-series measurements, AAR could also be utilised prior to any U-analyses for age-screening in locations where relative age information is required from multiple, poorly stratified reefs. Furthermore, amino acid analyses may also ultimately provide a tool for diagenetic screening prior to any U-analyses, but further study is required to determine the sensitivity of AA data to calcite concentration, relative to the detection limits of traditional XRD screening.

The most reliable U-series ages from the fossil specimen suggest that Foul Bay, on the SE coast of Barbados represents one of only two locations known to contain coral reefs that formed during the climatically important MIS 6.5, and records a sea level of -35 ± 7 msl at 165 ± 8 ka. Given that the other site is located on the west coast of Barbados, correlation between the two could also provide information regarding differential rates of tectonic movement.

ACKNOWLEDGMENTS

The authors would like to thank Prof. Ulrich Radtke (Dept. of Physical Geography, University of Cologne) for providing the fossil *A. palmata* sample, Remmert Shoutan, Stuart Kearns and Ben Buse, for providing useful instructions on microscopy, Simon Powell for advice on image preparation, Annabel Hodge for assistance with the kinetic experiments, Laura Robinson and David Richards for access to cutting equipment and Elizabeth Gladfelter for useful discussion. Also thanks are given to Sean Davis for conducting XRD analyses and Antony Burnham and Simon Kohn who performed Raman microspectroscopy. We thank Chris Coath (Bristol Isotope Group) and Richard Allen, Bea Demarchi and Sheila Taylor (BioArCh) for their assistance in the laboratory. AAR was undertaken with support from the Leverhulme Trust. PJT was supported by Alex Wilmot-Sitwell, the Wingate Foundation, the Natural History Museum London, and a UK Natural Environment Research Council postgraduate studentship (NERC DTG/GELYSN1402.6625). The authors thank Claudine Stirling for her careful editorial handling and the anonymous reviewer for the valuable comments that helped improve our manuscript.

APPENDIX A. SUPPLEMENTARY DATA

Supplementary data associated with this article can be found, in the online version, at http://dx.doi.org/10.1016/j.gca.2016.03.030.

REFERENCES

Allemand D., Tambutté E., Girard J. and Jaubert J. (1998) Organic matrix synthesis in the scleractinian coral *Stylophora pistillata*: role in biomineralization and potential target of the organotin tributyltin. *J. Exp. Biol.* **201**, 2001–2009.

Andersen M. B., Stirling C. H., Porcelli D., Halliday A. N., Andersson P. S. and Baskaran M. (2007) The tracing of riverine U in Arctic seawater with very precise $^{234}U/^{238}U$ measurements. *Earth Planet. Sci. Lett.* **259**, 171–185.

Andersen M. B., Stirling C. H., Potter E.-K., Halliday A. N., Blake S. G., McCulloch M. T., Ayling B. F. and O'Leary M. J. (2008) High-precision U-series measurements of more than 500,000 year old fossil corals. *Earth Planet. Sci. Lett.* **265**, 229–245.

Andersen M. B., Stirling C. H., Potter E.-K., Halliday A. N., Blake S. G., McCulloch M. T., Ayling B. F. and O'Leary M. J. (2010a) The timing of sea-level high-stands during Marine Isotope Stages 7.5 and 9: constraints from the uranium-series dating of fossil corals from Henderson Island. *Geochim. Cosmochim. Acta* **74**, 3598–3620.

Andersen M., Stirling C., Zimmermann B. and Halliday A. (2010b) Precise determination of the open ocean $^{234}U/^{238}U$ composition. *Geochem. Geophys. Geosyst.* **11**, Q12003.

Andersen M. B., Vance D., Keech A. R., Rickli J. and Hudson G. (2013) Estimating U fluxes in a high-latitude, boreal post-glacial setting using U-series isotopes in soils and rivers. *Chem. Geol.* **354**, 22–32.

Andersen M. B., Elliott T., Freymuth H., Sims K. W., Niu Y. and Kelley K. A. (2015) The terrestrial uranium isotope cycle. *Nature* **517**, 356–359.

Bada J. L. (1972) The dating of fossil bones using the racemization of isoleucine. *Earth Planet. Sci. Lett.* **15**, 223–231.

Bard E., Hamelin B. and Fairbanks R. G. (1990) U–Th ages obtained by mass spectrometry in corals from Barbados: sea level during the past 130,000 years. *Nature* **346**, 456–458.

Bard E., Antonioli F. and Silenzi S. (2002) Sea-level during the penultimate interglacial period based on a submerged stalagmite from Argentarola Cave (Italy). *Earth Planet. Sci. Lett.* **196**, 135–146.

Bar-Matthews M., Wasserburg G. J. and Chen J. H. (1993) Diagenesis of fossil coral skeletons: correlation between trace elements, textures, and $^{234}U/^{238}U$. *Geochim. Cosmochim. Acta* **57**, 257–276.

Berger A. L. (1978) Long-term variations of caloric insolation resulting from the Earth's orbital elements. *Quat. Res.* **9**, 139–167.

Brinton K. L. F. and Bada J. L. (1995) Comment on "Aspartic acid racemization and protein diagenesis in corals over the last 350 years". *Geochim. Cosmochim. Acta* **59**, 415–416.

Broecker W. S. (1963) A preliminary evaluation of uranium series inequilibrium as a tool for absolute age measurement on marine carbonates. *J. Geophys. Res.* **68**(9), 2817–2834.

Broecker W. S., Thurber D. L., Goddard J., Ku T. L., Matthews R. K. and Mesolella K. J. (1968) Milankovitch hypothesis supported by precise dating of coral reefs and deep-sea sediments. *Science* **159**, 297–300.

Brooks A. S., Hare P. E., Kokis J. E., Miller G. H., Ernst R. D. and Wendorf F. (1990) Dating Pleistocene archeological sites by protein diagenesis in ostrich eggshell. *Science* **248**, 60–64.

Chabaux F., Riotte J. and Dequincey O. (2003) U–Th–Ra fractionation during weathering and river transport. In *Rev. Mineral. and Geochem.*, 52 (eds. B. Bourdon, G. Henderson, C. Lundstrom and S. Turner). Elsevier, pp. 533–576.

Cheng H., Edwards R. L., Hoff J., Gallup C. D., Richards D. A. and Asmerom Y. (2000) The half-lives of uranium-234 and thorium-230. *Chem. Geol.* **169**, 17–33.

Cheng H., Edwards R. L., Shen C., Polyak V. J., Asmerom Y., Woodhead J., Hellstrom J., Wang Y., Kong X., Spötl C., Wang X. and Alexander, Jr., E. C. (2013) Improvements in ^{230}Th dating, ^{230}Th and ^{234}U half-life values, and U–Th isotopic measurements by multi-collector inductively coupled plasma mass spectrometry. *Earth Planet. Sci. Lett.* **371–372**, 82–91.

Clark P. U., Mitrovica J. X., Milne G. A. and Tamisiea M. E. (2002) Sea-level fingerprinting as a direct test for the source of global meltwater pulse IA. *Science* **295**, 2438–2441.

Collins M. J., Waite E. R. and van Duin A. C. T. (1999) Predicting protein decomposition: the case of aspartic-acid racemization kinetics. *Phil. Trans. R. Soc. B* **354**, 51–64.

Constantz B. R. (1986) The primary surface of corals and variations in their susceptibility to diagenesis. In *Diagenesis of Reefs* (eds. J. H. Schroeder and B. H. Purser). Springer, Berlin, pp. 53–76.

Constantz B. R. and Weiner S. (1988) Acidic macromolecules associated with the mineral phase of Scleractinian coral skeletons. *J. Exp. Zool.* **248**, 253–258.

Cross T. S. and Cross B. W. (1983) U, Sr and Mg in Holocene and Pleistocene corals *A. palmata* and *M. annularis*. *J. Sediment. Petrol.* **53**, 587–594.

Cuif J. P., Dauphin Y. and Gautret P. (1999) Compositional diversity of soluble mineralizing matrices in some recent coral skeletons compared to fine-scale growth structures of fibres: discussion of consequences for biomineralization and diagenesis. *Int. J. Earth Sci.* **88**, 582–592.

Cusack M., England J., Dalbeck P., Tudhope A., Fallick A. and Allison N. (2008) Electron backscatter diffraction (EBSD) as a tool for detection of coral diagenesis. *Coral Reefs* **27**, 905–911.

Downs R. (2006) The RRUFF project: an integrated study of the chemistry, crystallography, Raman and infrared spectroscopy of minerals. In *Program and Abstracts of the 19th General Meeting of the International Mineralogical Association in Kobe,*

Japan, pp. 3–13. Program and Abstracts of the 19th General Meeting of the International Mineralogical Association in Kobe, Japan.

Dullo W. C. (1987) The role of microarchitecture and microstructure in the preservation of taxonomic closely related scleractinians. *Facies* **16**, 11–22.

Edwards R. L., Chen J. H. and Wasserburg G. J. (1987) ^{238}U–^{234}U–^{230Th}–^{232}Th systematics and the precise measurement of time over the past 500,000 years. *Earth Planet. Sci. Lett.* **81**, 175–192.

Eggins S. M., Grün R., McCulloch M. T., Pike A. W., Chappell J., Kinsley L., Mortimer G., Shelley M., Murray-Wallace C. V., Spötl C. and Taylor L. (2005) In situ U-series dating by laser-ablation multi-collector ICPMS: new prospects for quaternary geochronology. *Quat. Sci. Rev.* **24**, 2523–2538.

Esat T. M. and Yokoyama Y. (2006) Variability in the uranium isotopic composition of the oceans over glacial–interglacial timescales. *Geochim. Cosmochim. Acta* **70**, 4140–4150.

Fruijtier C., Elliott T. and Schlager W. (2000) Mass-spectrometric ^{234}U–^{230}Th ages from the Key Largo Formation, Florida Keys, United States: constraints on diagenetic age disturbance. *Geol. Soc. Am. Bull.* **112**, 267–277.

Gallup C. D., Edwards R. L. and Johnson R. G. (1994) The timing of high sea levels over the past 200,000 years. *Science* **263**, 796–800.

Gallup C. D., Cheng H., Taylor F. W. and Edwards R. L. (2002) Direct determination of the timing of sea level change during Termination II. *Science* **295**, 310–313.

Gautret P., Cuif J. P. and Stolarski J. (2000) Organic components of the skeleton of scleractinian corals – evidence from in situ acridine orange staining. *Acta Palaeontol. Pol.* **45**, 107–118.

Gladfelter E. H. (1977) *Calcification and Productivity in a Dominant Shallow Water Reef Building Coral, Acropora palmata (Lamarck)* (M.S. thesis). University of the Pacific.

Gladfelter E. H. (1982) Skeletal development in *Acropora cervicornis*. I. Patterns of calcium carbonate accretion in the axial corallite. *Coral Reefs* **1**, 45–51.

Gladfelter E. H. (1984) A comparison of monthly rates of linear extension and calcium carbonate accretion measured over a year. *Coral Reefs* **3**, 51–57.

Gladfelter E. H. (2007) Skeletal development in *Acropora palmata* (Lamarck 1816): a scanning electron microscope (SEM) comparison demonstrating similar mechanisms of skeletal extension in axial versus encrusting growth. *Coral Reefs* **26**, 883–892.

Gladfelter E. H., Michel G. and Sanfelici A. (1989) Metabolic gradients along a branch of the reef coral *Acropora palmata*. *Bull. Mar. Sci.* **44**, 1166–1173.

Goodfriend G. A. (1991) Patterns of racemization and epimerization of amino acids in land snail shells over the course of the Holocene. *Geochim. Cosmochim. Acta* **55**, 293–302.

Goodfriend G. A. (1992) Rapid racemization of aspartic acid in mollusc shells and potential for dating over recent centuries. *Nature* **357**, 399–401.

Goodfriend G. A., Hare P. E. and Druffel E. R. M. (1992) Aspartic acid racemization and protein diagenesis in corals over the last 350 years. *Geochim. Cosmochim. Acta* **56**, 3847–3850.

Grant K. M., Rohling E. J., Ramsay C. B., Cheng H., Edwards R. L., Florindo F., Heslop D., Marra F., Roberts A. P., Tamisiea M. E. and Williams F. (2014) Sea-level variability over five glacial cycles. *Nat. Commun.* **5**, 5076–5090.

Gutner-Hoch E., Schneider K., Stolarski J., Domart-Coulon I., Yam R., Meiborn A., Shemesh A. and Levy O. (2016) Evidence for rhythmicity pacemaker in the calcification process of Scleractinian coral. *Sci. Rep.* **6**. http://dx.doi.org/10.1038/srep20191 20191.

Gvirtzman G., Friedman G. M. and Miller D. S. (1973) Control and distribution of uranium in coral reefs during diagenesis. *J. Sediment. Petrol.* **43**, 985–997.

Hamelin B., Bard E., Zindler A. and Fairbanks R. G. (1991) $^{234}U/^{238}U$ mass spectrometry of corals: how accurate is the U–Th age of the last interglacial period? *Earth Planet. Sci. Lett.* **106**, 169–180.

Hiess J., Condon D. J., McLean N. and Noble S. R. (2012) $^{238}U/^{235}U$ systematics in terrestrial uranium-bearing minerals. *Science* **335**, 1610–1614.

Henderson G. M. and Slowey N. C. (2000) Evidence from U–Th dating against Northern Hemisphere forcing of the penultimate deglaciation. *Nature* **404**, 61–66.

Henderson G. M., Cohen A. S. and O'Nions R. K. (1993) $^{234}U/^{238}U$ ratios and ^{230}Th ages for Hateruma Atoll corals: implications for coral digenesis and seawater $^{234}U/^{238}U$ ratios. *Earth Planet. Sci. Lett.* **115**, 65–73.

Hendy E. J., Gagan M. K., Lough J. M., McCulloch M. and de Menocal P. B. (2007) Impact of skeletal dissolution and secondary aragonite on trace element and isotopic climate proxies in Porites corals. *Paleoceanography* **22** PA4101.

Hendy E. J., Tomiak P. J., Collins M. J., Hellstron J., Tudhope A. W., Lough J. M. and Penkman K. E. H. (2012) Assessing amino acid racemization variability in coral intra-crystalline protein for geochronological applications. *Geochim. Cosmochim. Acta* **86**, 338–353.

Hill R. L. (1965) Hydrolysis of proteins. *Adv. Protein Geochem.* **20**, 37–107.

Hodge A. (2011) Establishing the relative chronology of raised reef terraces on Barbados using amino acid racemisation in fossilized *Acropora Palmata* corals. In *XVIII INQUA Congress, Bern, Switzerland (abstr.)*.

Hoffmann D. L., Prytulak J., Richards D. A., Elliott T., Coath C. D., Smart P. L. and Scholz D. (2007) Procedures for accurate U and Th isotope measurements by high precision MC-ICPMS. *Int. J. Mass Spectrom.* **264**, 97–109.

Husseini S. I. (1973) *Temporal and Diagenetic Modifications of the Amino Acid Composition of Pleistocene Coral Skeletons* (Ph.D. thesis). Brown University.

Ingalls A. E., Lee C. and Druffel E. R. M. (2003) Preservation of organic matter in mound-forming coral skeletons. *Geochim. Cosmochim. Acta* **67**, 2827–2841.

James N. P. (1974) Diagenesis of Scleractinian corals in the subaerial vadose environment. *J. Paleontol.* **48**, 785–799.

Kaufman D. S. and Manley W. F. (1998) A new procedure for determining DL amino acid ratios in fossils using reverse phase liquid chromatography. *Quat. Geochronol.* **17**, 987–1000.

Kaufman D. S. (2000) Amino acid racemization in ostracodes. In *Perspectives in Amino Acid and Protein Geochemistry* (eds. G. A. Goodfriend, M. J. Collins, M. L. Fogel, S. A. Macko and J. F. Wehmiller). Oxford University Press, pp. 145–160.

Kaufman D. S. (2006) Temperature sensitivity of aspartic and glutamic acid racemization in the foraminifera *Pulleniatina*. *Quat. Geochronol.* **1**, 188–207.

Kosnik M. A. and Kaufman D. S. (2008) Identifying outliers and assessing the accuracy of amino acid racemization measurements for geochronology. II. Data screening. *Quat. Geochronol.* **3**, 328–341.

Lajoie K. R., Wehmiller J. F. and Kennedy G. (1980) Inter- and intra-generic trends in apparent racemization kinetics of amino acids in quaternary molluscs. In *Biogeochemistry of Amino Acids* (eds. P. E. Hare, T. C. Hoering and K. J. King). Wiley, New York, pp. 305–340.

Lazar B., Enmar R., Schossberger M., Bar-Matthews M., Halicz L. and Stein M. (2004) Diagenetic effects on the distribution of

uranium in live and Holocene corals from the Gulf of Aqaba. *Geochim. Cosmochim. Acta* **68**, 4583–4593.

Lighty R. G., Macintyre I. G. and Stuckenrath R. (1982) *Acropora palmata* reef framework: a reliable indicator of sea level in the western Atlantic for the past 10,000 years. *Coral Reefs* **1**, 125–130.

Macintyre I. G. (1977) Distribution of submarine cements in a modern Caribbean fringing reef, Galeta Point, Panama. *J. Sediment. Petrol.* **47**, 503–516.

Miller G. H., Beaumont P. B., Jull A. J. T. and Johnson B. (1992) Pleistocene geochronology and paleothermometry from protein diagenesis in ostrich eggshells: implications for the evolution of modern humans. *Phil. Trans. R. Soc. B* **337**, 149–157.

Min G. R., Edwards R. L., Taylor F. W., Recy J., Gallup C. D. and Beck J. W. (1995) Annual cycles of U/Ca in coral skeletons and U/Ca thermometry. *Geochim. Cosmochim. Acta* **59**(10), 2025–2042.

Mitterer R. M. (1978) Amino acid composition and metal binding capability of the skeletal protein of corals. *Bull. Mar. Sci.* **28**, 173–180.

Nothdurft L. D. and Webb G. E. (2007) Microstructure of common reef-building coral genera *Acropora*, *Pocillopora*, *Goniastrea* and *Porites:* constraints on spatial resolution in geochemical sampling. *Facies* **53**, 1–26.

Nothdurft L. D. and Webb G. E. (2009) Earliest diagenesis in scleractinian coral skeletons: implications for palaeoclimate-sensitive geochemical archives. *Facies* **55**, 161–201.

Obert J. C., Scholz D., Felis T., Brocas W. M., Jochum K. P. and Andreae M. O. (2016) ^{230}Th/U dating of Last Interglacial brain corals from Bonaire (southern Caribbean) using bulk and theca wall material. *Geochim. Cosmochim. Acta* **178**, 20–40.

Penkman K. E. H., Preece R. C., Keen D. H., Maddy D., Schreve D. C. and Collins M. J. (2007) Testing the aminostratigraphy of fluvial archives: the evidence from intra-crystalline proteins within freshwater shells. *Quat. Sci. Rev.* **26**, 2958–2969.

Penkman K. E. H., Kaufman D. S., Maddy D. and Collins M. J. (2008) Closed-system behaviour of the intra-crystalline fraction of amino acids in mollusc shells. *Quat. Geochronol.* **3**, 2–25.

Penkman K. E. H., Preece R. C., Bridgland D. R., Keen D. H., Meijer T., Parfitt S. A., White T. S. and Collins M. J. (2011) A chronological framework for the British Quaternary based on Bithynia opercula. *Nature* **476**, 446–449.

Perrin C. (2004) Diagenèse précoce des biocristaux carbonatés: transformations isominérales de l'aragonite corallienne. *Bull. Soc. Géol. France* **175**, 95–106.

Perrin C. and Smith D. C. (2007) Earliest steps of diagenesis in living Scleractinian corals: evidence from ultrastructural pattern and Raman spectroscopy. *J. Sediment. Res.* **77**, 495–507.

Potter E.-K. and Lambeck K. (2004) Reconciliation of sea-level observations in the Western North Atlantic during the last glacial cycle. *Earth Planet. Sci. Lett.* **217**, 171–181.

Potter E.-K., Esat T. M., Schellmann G., Radtke U., Lambeck K. and McCulloch M. T. (2004) Suborbital-period sea-level oscillations during marine isotope substages 5a and 5c. *Earth Planet. Sci. Lett.* **225**, 191–204.

Potter E.-K., Stirling C. H., Andersen M. B. and Halliday A. N. (2005a) High precision Faraday collector MC-ICPMS thorium isotope ratio determination. *Int. J. Mass Spectrom.* **247**, 10–17.

Potter E.-K., Stirling C. H., Wiechert U. H., Halliday A. N. and Spötl C. (2005b) Uranium-series dating of corals in situ using laser-ablation MC-ICPMS. *Int. J. Mass Spectrom.* **240**, 27–35.

Robinson L. F., Adkins J. F., Fernandez D. P., Burnett D. S., Wang S.-L., Gagnon A. C. and Krakauer N. (2006) Primary U distribution in scleractinian corals and its implications for U series dating. *Geochem. Geophys. Geosyst.* **7**, Q05022.

Schellmann G. and Radtke U. (2004a) *The marine quaternary of Barbados*, Kölner Geographische Arbeiten No. 81, Geographisches Institut der Universität zu Köln.

Schellmann G. and Radtke U. (2004b) A revised morpho- and chronostratigraphy of the late and middle Pleistocene coral reef terraces on Southern Barbados (West Indies). *Earth Sci. Rev.* **64**, 157–187.

Scherer M. (1974) Submarine recrystallization of a coral skeleton in a Holocene Bahamian Reef. *Geology* **2**, 499–500.

Schindelin J., Arganda-Carreras I., Frise E., Kaynig V., Longair M., Pietzsch T., Preibisch S., Rueden C., Saalfeld S., Schmid B., Tinevez J.-Y., White D. J., Hartenstein V., Eliceiri K., Tomancak P. and Cardona A. (2012) Fiji: an open-source platform for biological-image analysis. *Nat. Methods* **9**, 676–682.

Scholz D. and Mangini A. (2007) How precise are U-series coral ages? *Geochim. Cosmochim. Acta* **71**, 1935–1948.

Scholz D., Mangini A. and Felis T. (2004) U-series dating of diagenetically altered fossil reef corals. *Earth Planet. Sci. Lett.* **218**, 163–178.

Scholz D., Mangini A. and Meischner D. (2007) U-Redistribution in fossil reef corals from Barbados, West Indies, and sea-level reconstruction for MIS 6.5. In *Developments in Quaternary Sciences, The climate of past interglacials* (eds. F. Sirocko, M. Claussen, M. Sanchez-Goni and T. Litt). Elsevier, New York, pp. 119–139.

Schroeder J. H. (1969) Experimental dissolution of calcium, magnesium, and strontium from recent biogenic carbonates: a model of diagenesis. *J. Sediment. Petrol.* **39**, 1057–1073.

Schroeder J. H., Miller D. S. and Friedman G. M. (1970) Uranium distributions in recent skeletal carbonates. *J. Sediment. Petrol.* **40**, 672–681.

Shen C.-C., Li K.-S., Sieh K., Natawidjaja D., Cheng H., Wang X., Edwards R. L., Lam D. D., Hsieh Y.-T., Fan T.-Y., Meltzner A. J., Taylor F. W., Quinn T. M., Chiang H.-W. and Kilbourne K. H. (2008) Variation of initial ^{230}Th/^{232}Th and limits of high precision U–Th dating of shallow-water corals. *Geochim. Cosmochim. Acta* **72**, 4201–4223.

Shirai K., Kawashima T., Sowa K., Watanabe T., Nakamori T., Takahata N., Amakawa H. and Sano Y. (2008) Minor and trace element incorporation into branching coral *Acropora nobilis* skeleton. *Geochim. Cosmochim. Acta* **72**, 5386–5400.

Speed R. C. and Cheng H. (2004) Evolution of marine terraces and sea level in the last interglacial, Cave Hill, Barbados. *Geol. Soc. Am. Bull.* **116**, 219–232.

Spooner P. T., Chen T., Robinson L. F. and Coath C. D. (2016) Rapid uranium-series age screening of carbonates by laser ablation mass spectrometry. *Quat. Geochronol.* **31**, 28–39.

Stirling C. H. and Andersen M. B. (2009) Uranium-series dating of fossil coral reefs: extending the sea-level record beyond the last glacial cycle. *Earth Planet. Sci. Lett.* **284**, 269–283.

Stirling C. H., Esat T. M., McCulloch M. T. and Lambeck K. (1995) High-precision U-series dating of corals from Western Australia and implications for the timing and duration of the Last Interglacial. *Earth Planet. Sci. Lett.* **135**, 115–130.

Stirling C. H., Esat T. M., Lambeck K. and McCulloch M. T. (1998) Timing and duration of the Last Interglacial: evidence for a restricted interval of widespread coral reef growth. *Earth Planet. Sci. Lett.* **160**, 745–762.

Stolarski J. (2003) Three-dimensional micro- and nanostructural characteristics of the scleractinian coral skeleton: a biocalcification proxy. *Acta Palaeontol. Pol.* **48**(4), 497–530.

Sykes G., Collins M. and Walton D. (1995) The significance of a geochemically isolated intracrystalline organic fraction within biominerals. *Org. Geochem.* **23**, 1059–1065.

Thompson W. G. and Goldstein S. L. (2005) Open-system coral ages reveal persistent suborbital sea-level cycles. *Science* **308**, 401–404.

Thompson W. G., Spiegelman M. W., Goldstein S. L. and Speed R. C. (2003) An open-system model for U-series age determinations of fossil corals. *Earth Planet. Sci. Lett.* **210**, 365–381.

Thompson W. G., Curran H. A., Wilson M. A. and White B. (2011) Sea-level oscillations during the last interglacial highstand recorded by Bahamas corals. *Nat. Geosci.* **4**, 684–687.

Tomiak P. K. (2013) *The Nature and Geochronological Applications of Coral Skeleton and Intra-crystalline Amino Acids* (Ph.D. thesis). University of Bristol.

Tomiak P. J., Penkman K. E. H., Hendy E. J., Demarchi B., Murrells S., Davis S. A., McCullagh P. and Collins M. J. (2013) Testing the limitations of artificial protein degradation kinetics using known-age massive *Porites* coral skeletons. *Quat. Geochronol.* **16**, 87–109.

Vallentyne J. R. (1964) Biogeochemistry of organic matter. II. thermal reaction kinetics and transformation products of amino compounds. *Geochim. Cosmochim. Acta* **28**, 157–188.

Villemant B. and Feuillet N. (2003) Dating open systems by the ^{238}U–^{234}U–^{230}Th method: application to quaternary reef terraces. *Earth Planet. Sci. Lett.* **210**, 105–118.

Wallace C. C. (1999) *Staghorn Corals of the World: A Revision of the Coral Genus Acropora*. CSIRO publishing Collingwood, Australia.

Wehmiller J. F. and Miller G. H. (2000) Quaternary geochronology: methods and applications. In *Aminostratigraphic Dating Methods in Quaternary Geology* (eds. J. S. Noller, J. M. Sowers and W. R. Lettis). American Geophysical Union, Washington DC, pp. 187–222.

Wehmiller J. F., Hare P. E. and Kujala G. A. (1976) Amino acids in fossil corals: racemization (epimerization) reactions and their implications for diagenetic models and geochronological studies. *Geochim. Cosmochim. Acta* **40**, 763–776.

Wehmiller J. F., Harris W. B., Boutin B. S. and Farrell K. M. (2012) Calibration of amino acid racemization (AAR) kinetics in United States mid-Atlantic Coastal Plain Quaternary mollusks using $^{87}Sr/^{86}Sr$ analyses: evaluation of kinetic models and estimation of regional Late Pleistocene temperature history. *Quat. Geochronol.* **7**, 21–36.

Young S. D. (1971) Organic material from scleractinian coral skeletons. I. Variation in composition between several species. *Comp. Biochem. Physiol. B Biochem. Mol. Biol.* **40B**, 113–120.

Associate editor: Claudine Stirling